PONTIFÍCIA UNIVERSIDADE CATÓLICA DO PARANÁ

ESCOLA POLITÉCNICA

PROGRAMA DE PÓS-GRADUAÇÃO EM ENGENHARIA MECÂNICA - PPGEM

ANDRE LUIZ ABOU HATEM

CARACTERIZAÇÃO TRIBOCORROSIVA, MECÂNICA E ESTRUTURAL DE REVESTIMENTOS NANOESTRUTURADOS DEPOSITADOS EM LIGA DE TITÂNIO PARA APLICAÇÕES BIOMÉDICAS

CURITIBA

2018

ANDRE LUIZ ABOU HATEM

CARACTERIZAÇÃO TRIBOCORROSIVA, MECÂNICA E ESTRUTURAL DE REVESTIMENTOS NANOESTRUTURADOS DEPOSITADOS EM LIGA DE TITÂNIO PARA APLICAÇÕES BIOMÉDICAS

Dissertação apresentada como requisito parcial à obtenção do grau de Mestre em Engenharia Mecânica, Curso de Pós-Graduação em Engenharia Mecânica, Escola Politécnica, Pontifícia Universidade Católica do Paraná.

Orientador: Prof. Dr. Paulo C. Soares Jr.
Coorientador: Prof. Dr. Ricardo D. Torres

CURITIBA

2018

Pontifícia Universidade Católica do Paraná
Escola Politécnica
Programa de Pós-Graduação em Engenharia Mecânica
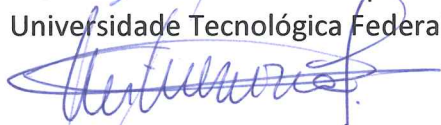
PUCPR
GRUPO MARISTA

TERMO DE APROVAÇÃO

André Luiz Abou Hatem

Caracterização Tribocorrosiva, Mecânica e Estrutural de Revestimentos Nanoestruturados Depositados em Liga de Titânio para Aplicações Biomédicas

Dissertação aprovada como requisito parcial para obtenção do grau de Mestre no Curso de Mestrado em Engenharia Mecânica, Programa de Pós-Graduação em Engenharia Mecânica, da Escola Politécnica da Pontifícia Universidade Católica do Paraná, pela seguinte banca examinadora:
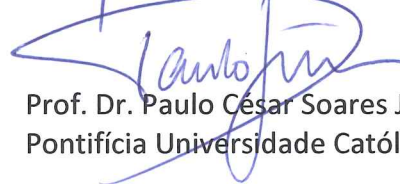
Prof. Dr. Carlos Maurício Lepienski
Universidade Tecnológica Federal do Paraná

Prof.ª Drª Michelle Sostag Meruvia
Pontifícia Universidade Católica do Paraná

Prof. Dr. Ricardo Diego Torres
Pontifícia Universidade Católica do Paraná, Co- Orientador

Prof. Dr. Paulo César Soares Junior
Pontifícia Universidade Católica do Paraná, Orientador

Curitiba, 16 de março de 2018

Eu dedico este trabalho ao meu pai, Elias Aziz Abou Hatem Filho, minha mãe, Sonia Aurea Abou Hatem e minha esposa, Mariana Midory Abe, por me proporcionarem as condições para que eu atingisse esta etapa.

"Adopt as your fundamental creed that you will equip yourself for life, not solely for your own benefit but for the benefit of the whole community."
Sir John Monash, 1923
(Serle, 1982, p. 481)

RESUMO

O comportamento tribocorrosivo insatisfatório verificado em aplicações biomédicas de titânio e ligas no corpo humano tem sido considerado como principal limitador da vida útil de próteses ortopédicas. As falhas a longo prazo nestes implantes estão associadas à produção de partículas de desgaste originadas de um processo de tribocorrosão atuante nas superfícies de interface dos componentes da prótese. Deposições de revestimentos finos duros com baixo coeficiente de atrito sob o titânio e ligas têm sido sugeridos como uma solução promissora para atender à demanda de vida útil destes componentes. Estes revestimentos podem consistir de materiais cerâmicos ou compósitos nanoestruturados com características auto lubrificantes e elevada resistência mecânica, dentre eles, o diamante-tipo carbono (DLC) e o carbonitreto de titânio e silício (TiSiCN). Desta maneira, este estudo tem como objetivo caracterizar o comportamento tribocorrosivo, a adesão e as propriedades mecânicas e estruturais de revestimentos finos diamante-tipo carbono (DLC) e nanocompósitos Ti(Si)CN depositados em liga de titânio ASTM F136 (Ti-6Al-4V), sob diferentes condições para a otimização de sua estrutura para o uso em aplicações biomédicas. Os revestimentos deste estudo foram obtidos por técnicas avançadas de deposição química e física de vapor assistidas por plasma, sendo respectivamente, "plasma immersion ion deposition" (PIID) e "plasma electron magnetron sputtering" (PEMS). Testes de tribocorrosão com deslizamento recíproco em solução tampão fosfato-salino (PBS) foram realizados em amostras de liga de titânio ASTM F136 revestidas com DLC e Ti(Si)CN e comparadas com amostras não revestidas. Além do comportamento tribocorrosivo das amostras revestidas, a morfologia, a estrutura e a composição químicas, as propriedades mecânicas e adesão dos revestimentos ao substrato também foram avaliadas. Os resultados demonstraram uma grande diminuição da taxa de desgaste nas amostras revestidas comparadas com as amostras de liga de titânio não revestida. A performance tribocorrosiva, a adesão e as propriedades mecânicas das amostras revestidas com DLC e Ti(Si)CN mostraram-se governadas por vários fatores atrelados a estrutura do revestimento, entre eles, a fração de ligações sp^2/sp^3 e o tamanho dos nanocristais de Ti(C)N, respectivamente. Além disso, as regiões amorfas de carbono presentes nos revestimentos se mostraram fundamentais na diminuição dos coeficientes de atrito observados. Em conclusão, os revestimentos nanoestruturados de baixo coeficiente de atrito estudados se confirmaram como alternativas para aumentar a performance tribocorrosiva, e assim, ampliar a vida útil de implantes ortopédicos de titânio.

Palavras-chave: Tribocorrosão, Revestimentos nanoestruturados, Liga de titânio, TiSiCN, DLC, Propriedades mecânicas, Adesão.

LISTA DE ABREVIATURAS E SIGLAS

ABCM	Associação Brasileira de Engenharia e Ciências Mecânicas
ASTM	American Society for Testing and Materials
COF	Coefficient of friction
DLC	Diamond-like carbon
HMDSN	Hexametildisilazano
p.	Página
PEMS	Plasma Enhanced Magnetron Sputtering
PIID	Plasma Immersion Ion Deposition
PPGEM	Programa de Pós-Graduação em Engenharia Mecânica
PUCPR	Pontifícia Universidade Católica do Paraná
SEM	Scanning Electron Microscopy
SwRI	SouthWest Research Institute
TMS	Trimetilsilano
XPS	X-ray photoelectron spectroscopy
XRD	X-ray diffraction

LISTA DE FIGURAS

Figuras - Artigo 2

LISTA DE TABELAS

SUMÁRIO

1 INTRODUÇÃO

O presente trabalho refere-se à caracterização tribocorrosiva, mecânica e estrutural de revestimentos nanoestruturados sob a liga de titânio ASTM F136 (Ti-6Al-4V), comumente empregada em implantes ortopédicos sujeitos à carga como as próteses de quadril, joelho e tornozelo. Ligas de titânio têm sido utilizado a estas aplicações devido sua elevada resistência à tração e compressão, baixa massa específica, alta resistência à corrosão e melhor biocompatibilidade quando comparado as outras alternativas comuns como as ligas de cobalto-cromo (Co-Cr) e os aços inoxidáveis.

Apesar da ampla utilização, as ligas de titânio apresentam um comportamento tribocorrosivo insatisfatório em próteses, muitas vezes, exigindo procedimentos de revisão complexos e dolorosos aos pacientes após 15 a 20 anos da instalação do implante (Desai, Bidanda e Bártolo, 2008; Gopal *et al.*, 2017). Estes procedimentos de revisão denominam-se artroplastias, que podem ser parciais, com a substituição de alguns componentes da prótese, ou ainda totais, com a remoção e inserção integral da prótese. Dentre os diagnósticos de artroplastias totais de revisão, o afrouxamento mecânico tem sido apontado como o mais recorrente em próteses de quadril, joelho e tornozelo (Herberts e Malchau, 2000; Robertsson *et al.*, 2001; Sadoghi *et al.*, 2013). Este diagnóstico ainda se agrava com o aumento do contingente populacional, da expectativa de vida e do nível de atividade da população. Apenas nos Estados Unidos, é esperado um acréscimo de 3,48 milhões e 572 mil no número de artroplastias de revisão total de joelho e quadril, respectivamente, até 2030 (Kurtz *et al.*, 2007).

O afrouxamento mecânico ocorre quando a prótese perde sua fixação ideal com o tecido ósseo, ocasionando um deslocamento acentuado de seus componentes, o que proporciona desconforto e dores ao paciente a curto prazo e a limitação do movimento restabelecido pelo implante a longo prazo. A origem do afrouxamento mecânico está associada à uma absorção óssea circundante ao implante, a qual é comumente desencadeada por um processo inflamatório gerado por partículas de desgaste derivadas das superfícies em contato da prótese imersas no fluido corporal (Raphel *et al.*, 2016). Uma vez que estas partículas metálicas são soltas na interface da prótese com o tecido ósseo, estas são atacadas pelo sistema imunológico, gerando o processo inflamatório responsável pela reabsorção óssea local.

Além disso, no caso de próteses de liga de titânio ASTM F136, o processo de degaste leva à dissolução de íons dos elementos estabilizadores das fases presentes no material, como alumínio e vanádio, cujo são apontados como causas de disfunções neurológicas e efeitos

citotóxicos no corpo humano (Geetha *et al.*, 2009; Hallab *et al.*, 2005; Sargeant e Goswami, 2006). Desta forma, uma melhora na performance tribocorrosiva das superfícies de liga de titânio é um objetivo crucial na prevenção de falhas de longo prazo em aplicações biomédicas e na diminuição do risco de doenças aos pacientes.

Dentre as modificações superficiais biocompatíveis existentes, revestimentos finos duros de baixo coeficiente de atrito (COF) tem-se mostrado promissores para aplicações ortopédicas. Estes revestimentos podem apresentar nanoestruturas que asseguram elevada dureza aliada a características de auto lubrificação importantes para uma boa resistência ao desgaste por deslizamento. Um exemplo é o carbono tipo diamante (DLC), com uma estrutura amorfa composta por ligações hibridizadas de carbono sp^2 e sp^3 que fornecem uma alta dureza (10 a 30 GPa), baixo coeficiente de atrito (0,05 a 0,2 em deslizamento na atmosfera contra grande parte dos materiais utilizados em implantes), biocompatibilidade e inércia química (Grill, 1999; Hauert, 2008; Robertson, 2002). No entanto, a baixa força de adesão limita a aplicação deste revestimento no campo biomédico. As altas tensões residuais introduzidas durante a deposição do filme podem causar delaminação extensa em materiais revestidos com DLC sob cargas críticas.

No entanto, outros materiais com estrutura otimizada e baixo COF também têm sido propostos nas superfícies dos componentes de próteses, tais como o carbeto de silício (SiC), o nitreto de titânio (TiN), o diboreto de titânio (TiB$_2$), o carbonitreto de titânio (TiCN), o nitreto de titânio e alumínio (TiAlN), o nitreto de cromo (CrN), o carbonitreto de cromo (CrCN) e recentemente, o quaternário carbonitreto de titânio e silício (TiSiCN) (McEntire e Lakshminarayanan, 2015).

Além da melhora das propriedades mecânicas e resistência à corrosão, a redução acentuada da taxa de desgaste em testes de tribocorrosão de superfícies revestidas com estes materiais têm sido atribuída à formação de uma camada de transferência de material, como o carbono que atua como lubrificante sólido no par tribológico (Erdemir *et al.*, 1996; Manhabosco e Müller, 2009; Wang *et al.*, 2017; Xu, Nie e Wei, 2006).

Presente a estas alternativas, faz-se necessário uma avaliação do comportamento tribocorrosivo destes revestimentos a fim de se otimizar suas estruturas para a aplicação em meio biológico. Adicionalmente, a adesão adequada destes revestimentos propostos ao material do implante torna-se também uma preocupação fundamental para se evitar falhas do revestimento, como delaminações que possam expor o substrato durante o uso. Portanto, a caracterização tribocorrosiva, mecânica e estrutural de revestimentos nanoestruturados propostos para a aplicação biomédica se faz essencial para o desenvolvimento de próteses de

liga de titânio revestidas que possam atender à demanda por uma vida útil prolongada de seus componentes.

1.1 OBJETIVOS

1.1.1 Objetivo geral

Caracterizar o comportamento tribocorrosivo, a adesão e as propriedades mecânicas e estruturais de revestimentos finos carbono tipo-diamante (DLC) e nanocompósitos Ti(Si)CN depositados em liga de titânio ASTM F136 (Ti-6Al-4V), sob diferentes condições de deposição para a otimização de sua estrutura para o uso em aplicações biomédicas.

1.1.2 Objetivos específicos

(a) Avaliar como a fração de ligações sp^2/sp^3 afeta o comportamento tribocorrosivo, a adesão e as propriedades mecânicas e estruturais de revestimentos finos DLC depositados em liga de titânio ASTM F136;

(b) Avaliar como as quantidades de carbono e silício presentes nos revestimentos afetam o comportamento tribocorrosivo, a adesão e as propriedades mecânicas e estruturais de revestimentos finos Ti(Si)CN depositados em liga de titânio ASTM F136;

(c) Verificar os índices (H/E) e (H^3/E^2) ligados a resistência ao desgaste dos revestimentos finos DLC e Ti(Si)CN depositados em liga de titânio ASTM F136;

(d) Comparar o potencial de circuito aberto (OCP), o coeficiente de atrito (COF) e a taxa de desgaste dos revestimentos finos DLC e Ti(Si)CN depositados em liga de titânio ASTM F136 com a liga de titânio ASTM F136 não revestida.

2 ESTRUTURA DA TESE

A figura 1 demonstra a estrutura final da dissertação de mestrado. Os elementos textuais deste trabalho serão, em parte, apresentados em formato de artigos conforme previsto em Resolução no. 21/2014 – CONSUN, REF: Normas para Pós-Graduação Strico Sensu da PUCPR. Desta forma, os artigos que compõem esta dissertação devem apresentar o autor da tese de mestrado como primeiro autor e estar publicados em revista indexada como, no mínimo, Qualis A2 na área das Engenharias III da CAPES.

Os artigos constituintes deste trabalho estão publicados e disponíveis para acesso via na internet na revista Surface & Coatings Technology (ISSN: 0257-8972) da Elsevier. Para respeitar os direitos autorais sob o formato das publicações da editora da revista, o conteúdo dos artigos foi formatado e apresentado segundo padrões textuais de dissertação da PUCPR. Assim como os elementos pré-textuais e pós-textuais, uma introdução geral e considerações finais sobre o tema estudado também estão previstas na estrutura desta tese e seguem formato e padrões convencionais das demais dissertações da instituição PUCPR.
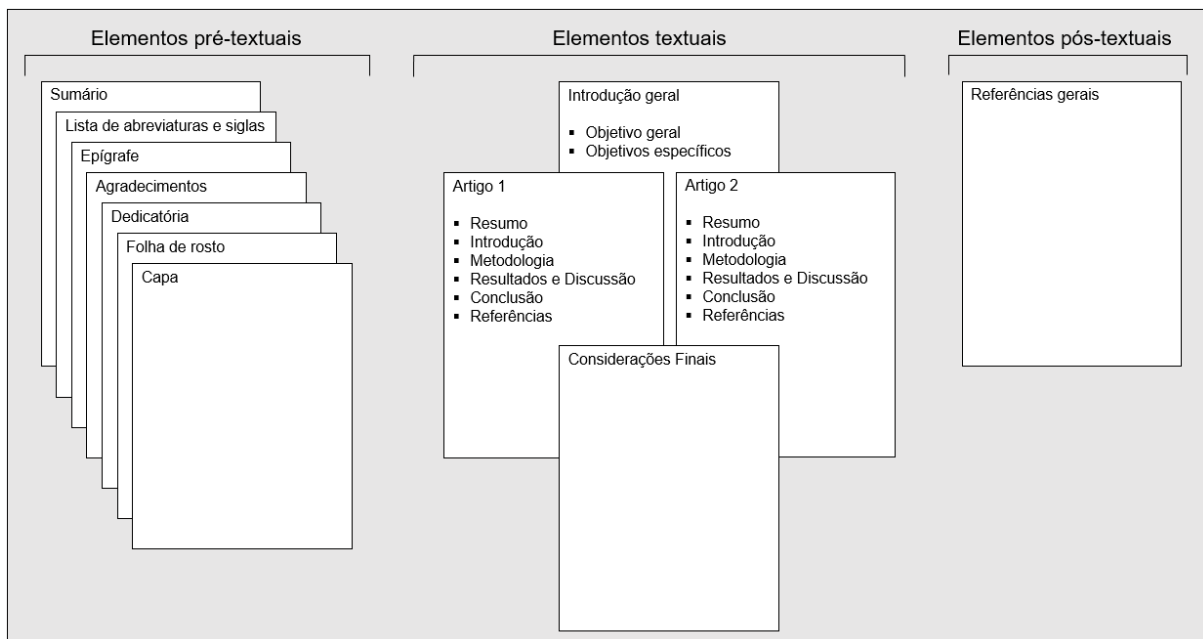
Figura 1 – Estrutura final da tese de mestrado com artigos compondo os elementos textuais.

3   **ARTIGO 1**

Tribocorrosion Behavior of DLC-Coated Ti-6Al-4V Alloy Deposited by PIID and PEMS+PIID Techniques for Biomedical Applications

Andre Hatem[a], Jianliang Lin[b], Rougha Wei[b], Ricardo D. Torres[a], Carlos Laurindo[a], Paulo Soares[a*]

[a] Department of Mechanical Engineering, Polytechnic School, Pontifícia Universidade Católica do Paraná, Curitiba, PR, 80215-901, Brazil.
[b] Surface Engineering & Materials Chemistry, Materials Engineering Department, Southwest Research Institute, San Antonio, TX, 78238, USA.

*Corresponding author
Paulo Soares, Prof. Dr.
Pontifícia Universidade Católica do Paraná
Polytechnic School - Mechanical Engineering Department
Rua Imaculada Conceição, 1155 – Prado Velho
ParqTec – Bl. 9
80215-901 Curitiba, PR – Brasil
+55 (41) 3271-1338
pa.soares@pucpr.br

Abstract

One of the main drawbacks observed from the usage of titanium alloys implants is the premature failures due to excessive wear and corrosion. Among the surface modification alternatives, Diamond-like carbon (DLC) coatings appear as a promisor candidate, since it has an amorphous structure chemically inert with desirable properties and still is a solid lubricant. Dense DLC coatings on biomaterials could be obtained by advanced vapor deposition techniques as the plasma immersion ion deposition (PIID) and the plasma enhanced magnetron sputtering (PEMS). This work aims to investigate the tribocorrosion behavior of DLC coatings systems, obtained by PIID only and PEMS+PIID hybrid techniques, applied on Ti-6Al-4V alloy samples for biomedical applications. The tribocorrosion tests were performed under phosphate-buffered saline (PBS) solution on the DLC-coated samples and compared to a Ti-6Al-4V bare alloy sample. Besides tribocorrosion tests, it were performed X-ray photoelectron spectroscopy (XPS), Raman spectroscopy, scanning electron microscopy (SEM), nanoindentation and scratch tests to evaluate the microstructure, morphology, mechanical properties and adhesion of the DLC-coated samples, respectively. The tribocorrosion tests demonstrated at least 5 times less friction coefficient and less than 2% of wear rate DLC-coated samples compared to Ti-6Al-4V bare alloy sample. Nevertheless, the results show that DLC coatings deposited by the advanced plasma enhanced techniques are very promissory to improve tribocorrosion behavior in Ti-6Al-4V alloy implants.

Keywords: Titanium alloy, DLC coatings, XPS, Raman spectroscopy, SEM, Adhesion, Hardness, Tribocorrosion

1. Introduction

One of the main drawbacks observed from the usage of titanium alloys implants is the premature failures due to excessive wear and corrosion. These often lead to a total revision arthroplasty caused by a range of diagnoses, with higher recurrence to infection, mechanical loosening, breakages, and dislocation. Among them, mechanical loosening was indicated as the most common reason for all component revision of hip implants in the procedures performed between 2009 and 2013 in the United States [1]. Although the mechanism inherent of mechanical loosening are still not fully understood, implant micromotions begin with a combination of macro-, micro- and nano- simultaneous events during loading [2]. Tribocorrosion process involving sliding and fretting corrosion under body fluids generate implant wear debris that lead the surrounding tissue to inflammatory reactions, bone resorption, and low implant osseointegration. These conditions may result in total revision arthroplasty due to mechanical loosening just after 10 to 20 years of placement procedure in bearing loading implants [3]. Also, tribocorrosion process may expose human body to noxious elements when they are present in the implant alloy composition. In the case of Ti-6Al-4V, an extensive titanium alloy used in the biomedical applications, vanadium ions released from the implant can generate cytotoxic reactions and neurological disorders in the patient [4]. The vanadium ions toxicity reactions may disfavor local cell regeneration contributing to poor osseointegration. Superior cellular attachment, proliferation, and response were found in vanadium-free titanium alloys in comparison of Ti-6Al-4V alloy [5], which highlights the ions releasing role in mechanical loosening prevention. Therefore, modifications on the implant surfaces to improve tribocorrosion behavior could be very promising to overcome mechanical loosening causes, especially on Ti-6Al-4V alloy implants.

Recently, new deposition techniques and coating compositions have been emerged targeting higher mechanical, microstructural and tribocorrosion properties on the implant surfaces. Diamond-like carbon (DLC) appears as a considerable coating option in this case since it has an amorphous structure chemically inert composed by two types of carbon hybridizations (sp2 and sp3) that provides an extreme hardness, low friction coefficient, biocompatibility and still, is a solid lubricant [6,7]. While diamond fraction (sp3 bond sites) grants an extreme hardness to DLC coating, the graphitic fraction (sp2 bond sites) contributes to low friction coefficient, which is generally between 0.05 to 0.2 in atmosphere against most implant counterpart materials. As a solid lubricant, a so-called transfer layer from graphitic fraction deposits onto counterpart, which prevents wear on counterpart and provides very low wear rates to the DLC coating under dry tribological conditions [8–11]. Moreover, the bonds

structure fraction in DLC coatings is also important because it can affect coating biological response. According to Liao et. al. [12], DLC coatings with superior sp3 content can maximize osteoblastogenesis and fibroblastic response and minimize inflammatory reactions due to less repulsive force finding on the implant surface. Nonetheless, not only the bonds fraction affects this behavior, but also the adhesion between coating and substrate to avoid its detachment [13], which in turn is strongly related to the applied deposition technique [14]. Moreover, carbide and nitride interlayers are often deposited over substrate favoring the DLC coatings adhesion [13–16]. Although these superior properties turn DLC coatings in a proper candidate to load bearing implants, they were mainly evaluated in air or vacuum environments, and still have to be more investigated in vitro and in vivo biomedical environments, where corrosion fluids may accelerate the wear process on DLC coatings. Manhabosco and Müller [17] have investigated the tribocorrosion behavior of DLC coatings deposited by Radio Frequency Plasma assisted chemical vapor deposition under PBS solution. The authors concluded that DLC coatings can have 10 times less lifetime in tribocorrosion environment compared to dry conditions. However, a recent study of Zhao et. al. [18] verified similar low wear rates for DLC coatings under dry and simulated body fluid compared to several metallic biomaterials. Accordingly, DLC coatings could present favorable tribocorrosion behavior for biomedical applications but it will heavily depend on how the coating is conceived and deposited on the pretended layer coating system.

Among the advanced DLC deposition techniques are the plasma immersion ion deposition (PIID) and the plasma enhanced magnetron sputtering (PEMS). Both are examples of the plasma enhancement during film vapor depositions that results in coatings with higher density and adhesion when compared to other conventional techniques [19]. In PIID technique DLC coatings can be produced with very high hardness (10-25 GPa) and thickness up to 2 µm using carbonaceous precursor, such as methane or acetylene, in a simpler and less expensive approach when compared to other conventional technique [20]. DLC produced by PEMS technique relies on sputtering discharges on pure carbon targets and hydrocarbons decomposition from a precursor by electron impact [21]. Although is still possible to deposit DLC by PEMS, the technique is more suitable to produce carbide and nitride interlayers prior a DLC PIID for biomedical coating systems. Therefore the use of combined techniques can generate a DLC coating system with desirable tribocorrosion behavior due to a higher adhesion between DLC, interlayer, and the substrate.

This work aims to investigate the tribocorrosion behavior of DLC coatings with distinct carbide and nitride interlayers, obtained by PIID only and PEMS+PIID hybrid techniques, applied on Ti-6Al-4V alloy samples.

2. Experimental Procedure

2.1. Coating depositions

Substrate samples were obtained in 2 mm thick discs from electron-erosion cutting of a Ti-6Al-4V ELI (ASTM F136) annealed bar with 25.4 mm diameter and prepared by conventionally grinding and polishing.

The PIID-DLC coating was deposited using Southwest Research Institute (SwRI) PIID deposition system, which consists of a cylindrical vacuum chamber with a diameter of 1.2 m and length of 2.4 m. The base pressure in the chamber was below 5×10^{-4} Pa. The substrates were installed in the middle of the chamber. The substrates were cleaned using an Ar glow discharge plasma generated by applying a negative pulse voltage on the substrates at a pressure of 2.67 Pa. After etch cleaning the substrates, a SiC bond layer was firstly deposited by introducing 20 sccm of tetramethylsilane (TMS) into the chamber. The pulsed voltage and current on the substrates were 6 kV and 100 A, respectively. The pulsing frequency was 500 Hz and the pulse width was 20 μs. Finally, the PIID-DLC coating was deposited on top of the SiC layer by introducing acetylene (C_2H_2) into the chamber at a flow rate of 80 sccm and a working pressure of 1.3 Pa for 120 minutes. More detailed description of the SwRI PIID-DLC deposition process and parameters can be found elsewhere [20].

The PEMS+PIID DLC coatings were deposited in a magnetron sputtering system equipped with two round balanced magnetrons (152 mm in diameter) facing one to another with a distance of 300 mm. A graphite target (99.5% purity) and a Ti metal target (99.95% purity) were installed in the chamber. The substrates were mounted on a double rotation holder, which rotated at a speed of 4 rpm in the center of the chamber. The chamber was pumped down to a base pressure below 5.0×10^{-4} Pa prior to all depositions. The substrates were ion cleaned at a bias voltage of -120 V with a global discharge current of 4.5 A which was generated by powering tungsten (W) filaments at 45 A using the plasma enhanced magnetron sputtering (PEMS) technique [22]. Once the substrate cleaning was finished, a Ti/TiN/TiC compositionally graded bond layer was deposited. After putting down the bond layers, the W filaments were turned off. Then C_2H_2 was fed into the chamber at a flow rate of 250 sccm, which resulted in a working pressure of 0.67 Pa. The substrate was biased using a pulsed dc power supply at a constant voltage of -650 V. The pulsing parameters include 100

kHz and 90% duty cycle. The pulsed voltage on the substrates generated glow discharge plasma in the chamber, which dissociated C_2H_2 and formed DLC coating on the substrates.

2.2 Samples Characterization

The surface morphologies and cross-sectional microstructures of DLC coatings were obtained by secondary electrons detection in scanning electron microscope (TESCAN VEGA3) at 20 kV. The coatings fraction between sp2 and sp3 bonds was assessed through Raman and X-ray photoelectron spectroscopy (XPS). Raman analyses were conducted using a confocal micro-Raman spectrometer with 514 nm frequency Argon ion laser. While XPS measurements were obtained with 1486.7 eV Al Kα X-ray excitation source and calibrated by the C1s peak at 284.8 eV. The bonds fraction was calculated from the ratio between the Gaussian fitting curve areas of XPS spectra removing the Shirley-type background. Nanoindentations were performed by ASMEC UNAT nanomechanical tester using quasi-continuous stiffness measurements (QCSM) method with a Berkovich diamond indenter to verify hardness and elastic modulus of the coatings. The indentations were set in three columns with three indentations each 75 µm equally spaced using a maximum load of 400 mN. Coatings adhesion were verified by scratch test following ASTM C1624-05 Standard [23] on a scratch tester from CSM Instruments. Three linear progressive load scratch test were performed on each sample using standard parameter values of 100 N/min loading rate, 10 mm/min horizontal displacement rate in a total scratch length of 5 mm resulting in final test load of 50 N. Then, two-level critical scratch load (Lc1 and Lc2) were assigned to the normal load value at the first appearance of cohesive and adhesion failures, which were identified using an optical microscope and classified according to the scratch atlas presented in the ASTM C1624-05 Standard. Moreover, acoustic emission and stylus tangential force signals were obtained as secondary test data to assist in failure identification. The coefficient of friction was determined as the ratio of tangential force to the normal force measured during the test. The depths of the scratch profiles were also registered during and after the test to the posterior evaluation of the coatings elastic recovery. In order to simulate a physiological human body environment, the tribocorrosion tests were conducted under phosphate-buffered saline (PBS) solution at 1X concentration. The electrolyte cell was set-up in a three electrode system, using an Ag/AgCl, NaCl (sat'd) as the reference electrode, a Pt wire as the counter electrode and the samples of DLC coatings and aTi-6Al-4V bare alloy sample as the working electrodes. The active exposed area of the samples to the electrolyte solution used was 0.36cm^2. The open circuit potentials (OCP) were monitored by a potentiostat (Ivium) during

the entire test. Firstly, samples were plunged in a vat with 700 ml of PBS for 1 hour to stabilize the OCP. Then, using a universal tribometer (Anton-Paar), reciprocal sliding test were performed with 2 mm amplitude at the maximum linear speed of 1 cm/s, applying a 10 N normal force and using a 6 mm diameter Al_2O_3 ball for a total distance of 10 meters. After the reciprocal sliding test, the samples were left for 30 minutes in the solution to allow any repassivation. Finally, images of wear tracks morphologies were obtained by scanning electron microscopy in secondary electron mode. The wear track profiles were examined by a contact profilometer integrated to the tribometer and the coatings wear rates were calculated trough the tribometer software with the coating volume losses (mm³) divided by the normal force (N) and the total sliding distance (m) applied on the test.

3. Results and discussion

3.1 Morphology

Figure 1 presents the surface and cross-section SEM images for the DLC coatings obtained by PIID and PEMS+PIID techniques. Both coatings exhibited typical cauliflower-like surface morphology from coatings deposited by plasma enhanced film vapor depositions [24–28]. The structures that composed the topography are not crystals but bonded amorphous carbon regions presented as nodules with different sizes. In the surface images of PEMS+PIID DLC coating were noticed some micro-cracks and more defined boundaries between nodules compared to PIID DLC coating. This difference was expected due to higher ion flux bombardment during PEMS+PIID DLC deposition [28].
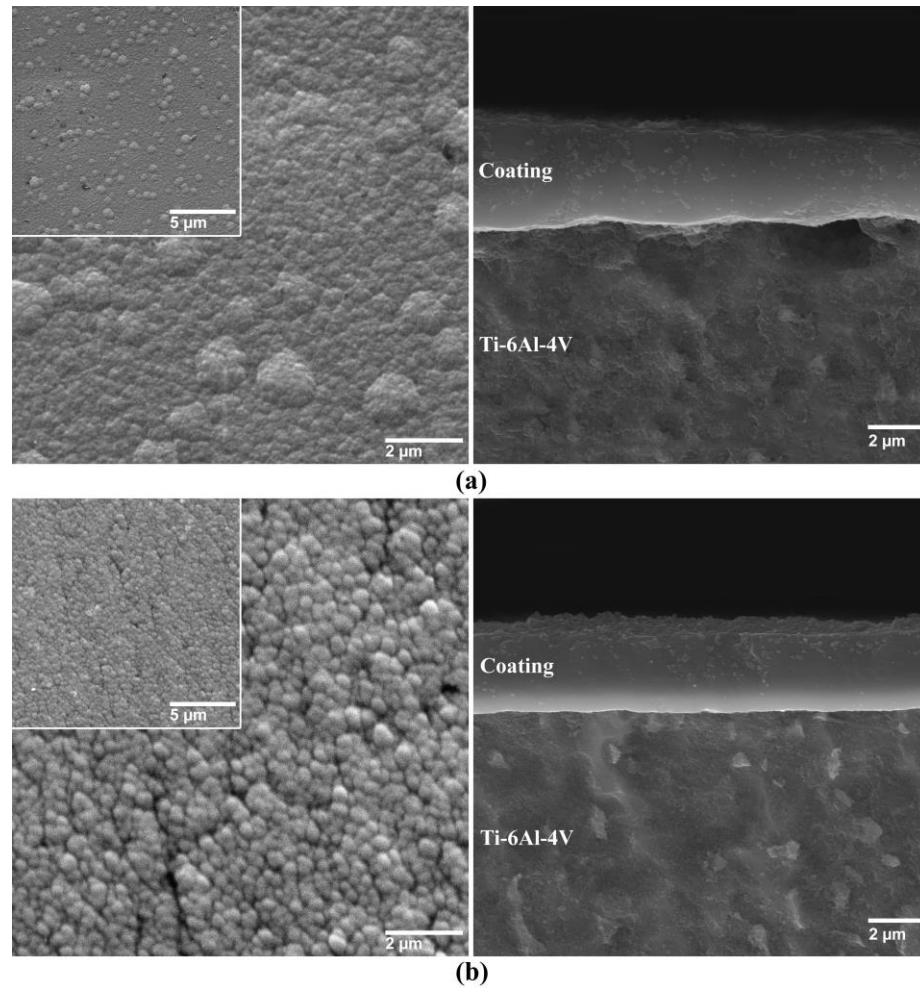
Figure 1 – Surface and cross-section SEM images by secondary electrons for the DLC coatings obtained by (a) PIID and (b) PEMS+PIID techniques.

Cross-section images demonstrate dense coatings with no growth structure formations and absence of boundaries between DLC film and the interlayers on both techniques. Gradients along the coating depth are perceived and attributed to the interlayers of the coating system. Therefore, due to no defined boundary between DLC and interlayers in SEM images, it was performed cross-sectional chemical composition analysis by energy dispersive X-ray spectroscopy (EDS) to obtain the DLC film thicknesses. In figure 2, the coating systems obtained by the both techniques reach total thicknesses of 5-6 µm and DLC films were detected by the first peak with higher counts of carbon presenting thicknesses between 1 to 2 µm.
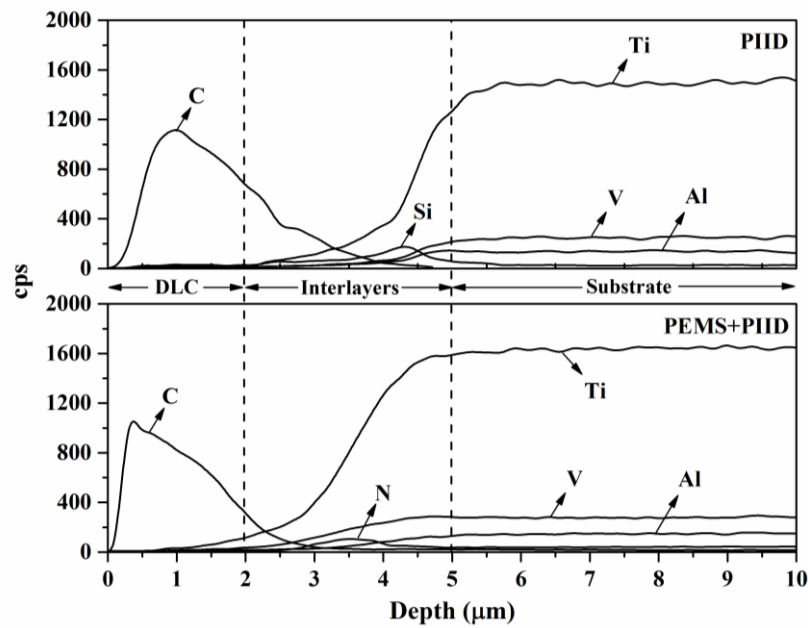
Figure 2 – Cross-sectional chemical composition DLC coatings with SiC interlayer obtained by PIID technique and DLC coating with Ti/TiN/TiC interlayers obtained by PEMS+PIID technique.

Also, the presence of interlayer chemical elements as Si and N could be verified for PIID and PEMS+PIID DLC coatings respectively. Thus, both DLC coating techniques generating higher density uniform coatings with similar thicknesses. The defects verified on the topography of PEMS+PIID DLC coating are mainly attributed to higher ion flux bombardment promoted by a greater acetylene flow rate used during this DLC deposition. The same reason is suggested to the smoother surface obtaining on PIID DLC coating.

3.2 Raman analyses

Figure 3 shows the Raman spectra of the DLC coatings obtained by PIID and PEMS+PIID techniques. The spectra reveal the typical amorphous carbon hydrogenated (a-C: H) coatings response of D and G bands that were deconvoluted by two Gaussian curves centered around 1375 cm^{-1} and 1546 cm^{-1} respectively. The peaks centering position are found in good agreement with other DLC Raman analyses with same frequency excitation source [29,30].
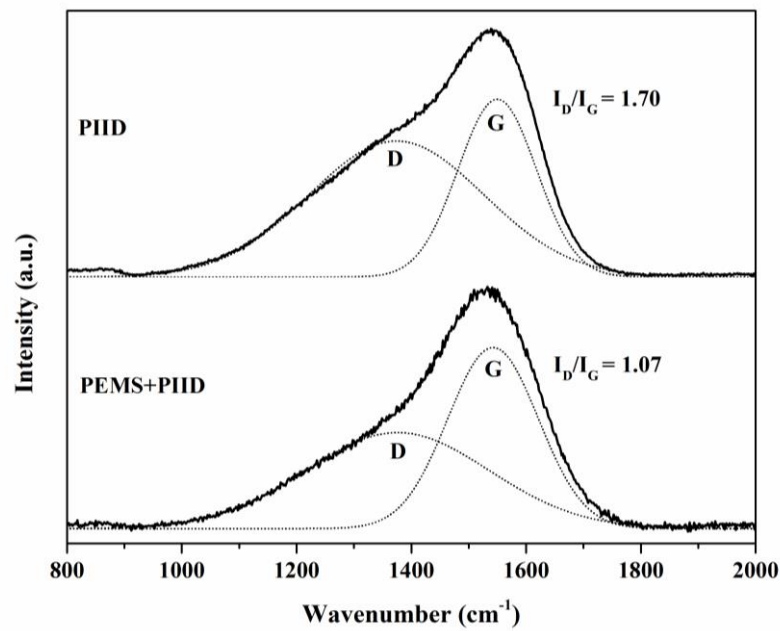
Figure 3 – Raman spectra with D and G fitting curves for the DLC coatings obtained by PIID and PEMS+PIID techniques.

The index I_D/I_G is often used to evaluate the disorder degree of DLC coatings, for instances, the D peak is the signed response from breathing mode of sp2 disordered carbon atoms in aromatic rings structure while G peak is resulted from stretching mode of sp2 disordered carbon atoms [31,32]. In Table 1 are presented the parameters of the Gaussian curves used to fitting D and G peaks for both DLC coatings. As shown, PEMS+PIID DLC coating presented a lower I_D/I_G with a slight left shift of G peak position when compared to PIID DLC coating which indicates higher sp3 content with a small distortion in sp2 carbon network [32]. The PEMS+PIID DLC coatings were obtained in a greater acetylene flow rate with a pulsing dc power which contributed to a higher hydrocarbon ion bombardment producing much more sp3 carbon hybridization and hydrocarbon stretching bonds in the deposited coating [33]. Although quantitative information about the sp3/sp2 fraction of a-C:H coatings might not be retrieved from Raman spectra, the analyses demonstrate relevant qualitative information which suggests the PEMS+PIID DLC closer to diamond-like behavior.

Table 2 - Raman spectra D and G peak parameters for the DLC coatings.

Coating deposition technique	D Peak		G Peak		I_D/I_G
	Position (cm⁻¹)	FWHM (cm⁻¹)	Position (cm⁻¹)	FWHM (cm⁻¹)	
PIID	1373.84	358.33	1549.70	161.01	1.70
PEMS+PIID	1376.13	375.20	1542.44	186.26	1.07

3.3 XPS

Figure 4 shows the C1s peaks from XPS spectrum for the DLC coatings obtained by PIID and PEMS+PIID techniques. The C1s peaks were fitted by three Gaussians curves centered at 284.3 eV, 285.3 eV and 287.3 eV for PIID DLC coating and 284.1 eV, 284.6 eV and 286.0 eV for PEM+PIID coating. These deconvolutions were attributed to C-C sp2, C-C sp3, and C=O bondings respectively, according to references [34–37]. The area ratio of sp2 and sp3 fitting curves were used to determine the fraction of sp3 bonding content on the DLC coatings. The almost double amount of sp3 bonding was found on the DLC coating obtained by PEMS+PIID technique compared to PIID technique. This result agreed with the lower I_D/I_G from Raman analyses on this coating and indicates that higher ion bombardment contributing to the formation of sp3 carbon hybridization during DLC deposition. The XPS also evinced presence of C=O bondings on coatings which may come from residual oxygen presenting on chamber during coating depositions.
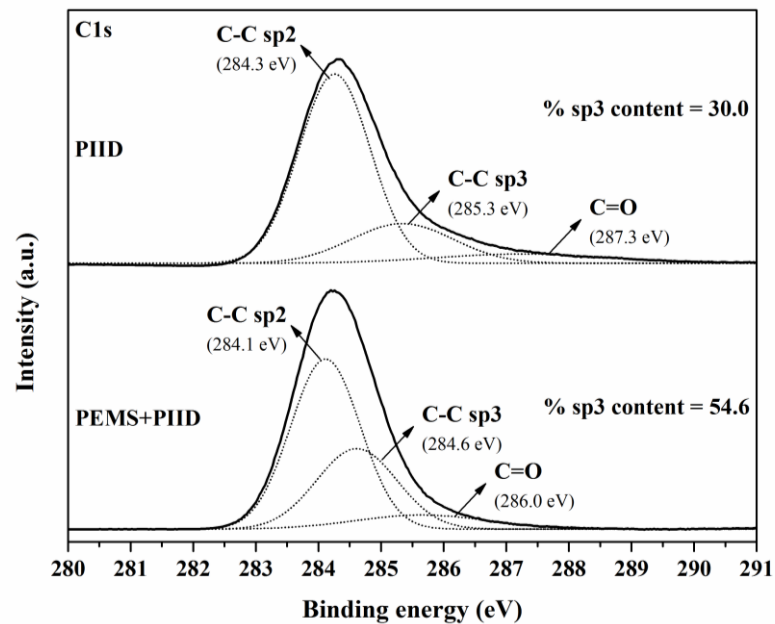
Figure 4 – XPS C1s peaks with Gaussian deconvolutions and %sp3 content for the DLC coatings obtained by PIID and PEMS+PIID techniques.

3.4 Mechanical properties

Figure 5 present hardness and elastic modulus as a function of indentation depth of the DLC coatings obtained by nanoindentation. On PEMS+PIID DLC coating the hardness firstly increased reaching a maximum mean value of 20.4 GPa at 0.13µm depth and then decreased with a gradually reducing on elastic modulus due to the effect of the substrate lower hardness. This behavior was not observed on PIID DLC coating which presented maximum mean hardness value of 7.7 GPa and kept constantly with elastic modulus along the coating. These values are found in good agreement with others plasma enhanced ion immersion DLC depositions [14,38,39]. Combined with Raman and XPS analyses, the increased mechanical properties presented by PEMS+PIID DLC coating regards to the higher amount of sp3 bonding sites presented on its structure. Normally in carbon films, higher hardness are related to the higher amount of sp3 bonding, higher densities and residual stresses [15,16]. In PIID DLC coatings, the substrate does not demonstrate depletion on the mechanical properties along the coating profile which suggests closer average values of hardness and elastic modulus between coating, interlayer, and the substrate. Besides the evaluation of hardness and elastic modulus individually, authors [40–42] declare the elastic strain to failure, which is determined by the H/E ratio, to be close correlated with relative wear resistance. Therefore, in order to verify the coating-substrate system wear resistance, the H/E ratio from both DLC coatings was evaluated taking into account only the hardness and elastic modulus beyond the 10% thickness of the coating. The average values found for the elastic strain to failure are 0.0871 and 0.0890 for the PIID and PEMS+PIID DLC samples respectively. From these results, a close relative wears resistance of the coating-substrate system could be expected for both coatings, even despite the gradient observed along the coating thicknesses of PEMS+PIID DLC sample.
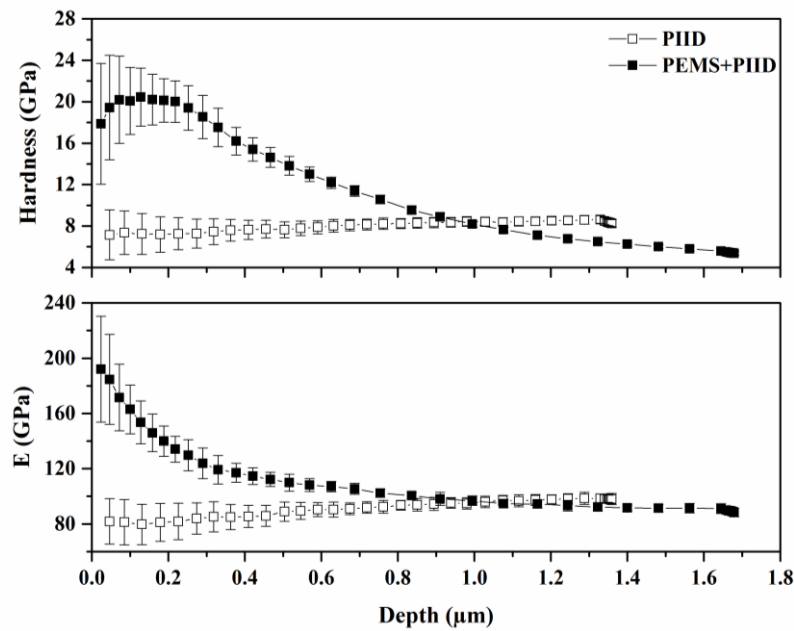
Figure 5 – Nanohardness and elastic modulus profile for the DLC coatings obtained by PIID and PEMS+PIID techniques.

3.5 Adhesion

The adhesion of the DLC coatings was examined by a scratch test which can quantitatively assess the adhesion strength in hard coatings by comparing critical loads (L_C). These critical loads are normally determined as the normal force correlated to the first appearance of cohesive and adhesive failures such as cracks and coating delamination. In this study, two-level critical scratch loads (L_{C1} and L_{C2}) were determined on the initial points of the cohesive and adhesive failures of the DLC coatings, which in turn were verified by optical microscopy assisted by tangential force and acoustic emission signals following the ASTM C1624-05 Standard [23]. Furthermore, the scratch depths during and after the test were analyzed in order to verify the elastic recovery from the DLC coatings to titanium substrate system. Therefore, figure 6 and 7 present the scratch optical images indexed to graphs with the monitored responses (tangential force, friction coefficient, acoustic emission, profile and residual depths) as a function of normal force and distance during a scratch test performed on a sample of PIID DLC and PEMS+PIID DLC respectively. In figure 6, the scratch test could be divided into three distinct regions. In the first region, which is prior to the first identified cohesive failure (left from the L_{C1} line), is observed an increase of a quivered friction coefficient with the linear progressive normal force. This is a common response from the asperities removal from the coating surface by the indenter and no significant variation from

the start acoustic emission signal could be detected in this region. Then, a second region could be defined by the first appearance of cohesive failure and before first adhesive failure (between L_{C1} and L_{C2} lines), where the friction coefficient continues to increase with a defined slope and some small variations on the acoustic emission data were detected by the recurrence of cohesive failures on the coating. Then, after the first appearance of adhesive failure (right from the L_{C2} line), a third region could be defined by a steep rise, on both, friction coefficient and acoustic emission values with high amplitude peaks until the end of the scratch test which are related to the regularly spaced spallation observed besides the scratch trail.
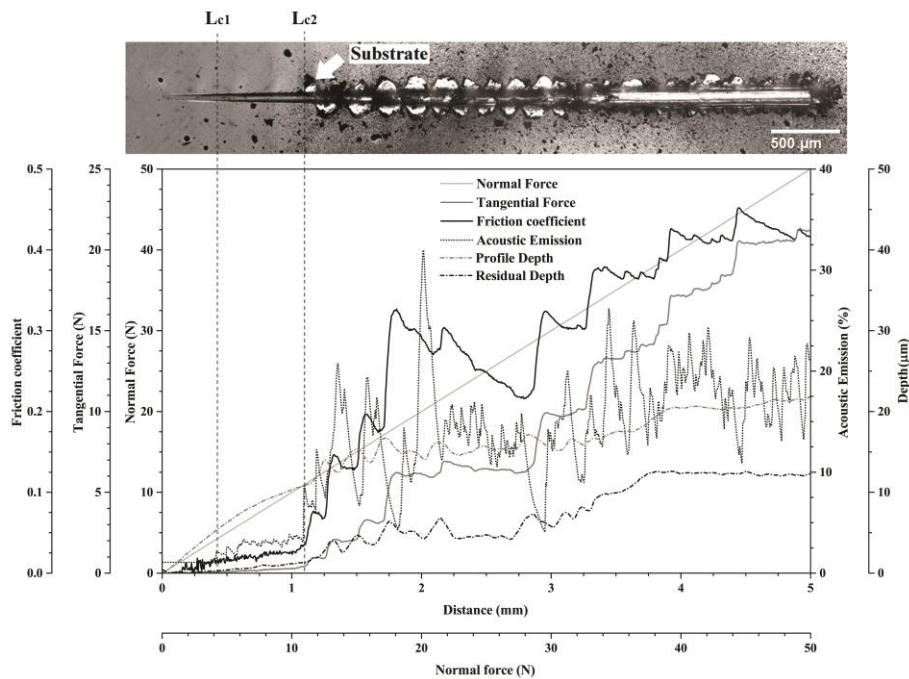
Figure 6 – Scratch test optical image indexed to the graph of monitored responses as a function of the applied normal force and scratch distance of the PIID DLC coating.

In figure 7, PEMS+PIID DLC scratch test presented similar three distinct regions on the graph as PIID DLC sample until 1.5 mm scratch distance. However, in this coating, no abrupt increase in friction coefficient could be observed after the L_{C2} line which could be attributed to the singular adhesive failure mode differentiate by the large area spallation around the scratch trail [43]. After the scratch distance of 1.5 mm, the graph presents the same acoustic emission values of the test start with a small linear increase in friction coefficient until reach the cohesive failures on TiC interlayer, at a 2 mm scratch distance. Further, adhesive failures between TiC interlayer and substrate were also observed around 2.7 mm. In order to quantitatively assess the adhesion strength of the DLC coatings, the critical loads

were assigned only by DLC layer failures, thus the failures between interlayers and substrate were unconsidered in the evaluation. Moreover, an elastic deformation of about 10µm could be observed on both DLC coating-substrate systems by comparing the profile and residual depths registered on the tests. These similar values were expected as the coatings demonstrated close values of H/E ratio [42]. In the case of PIID DLC sample, the elastic recovery mismatch between DLC coating and titanium substrate resulted in the spallation failure observed during the system relaxation after indenter traveling. While, in PEMS+PIID DLC, an extensive spallation occurred in the interface between DLC layer and TiC interlayer due to the demonstrated mechanical properties gradient inner this coating.
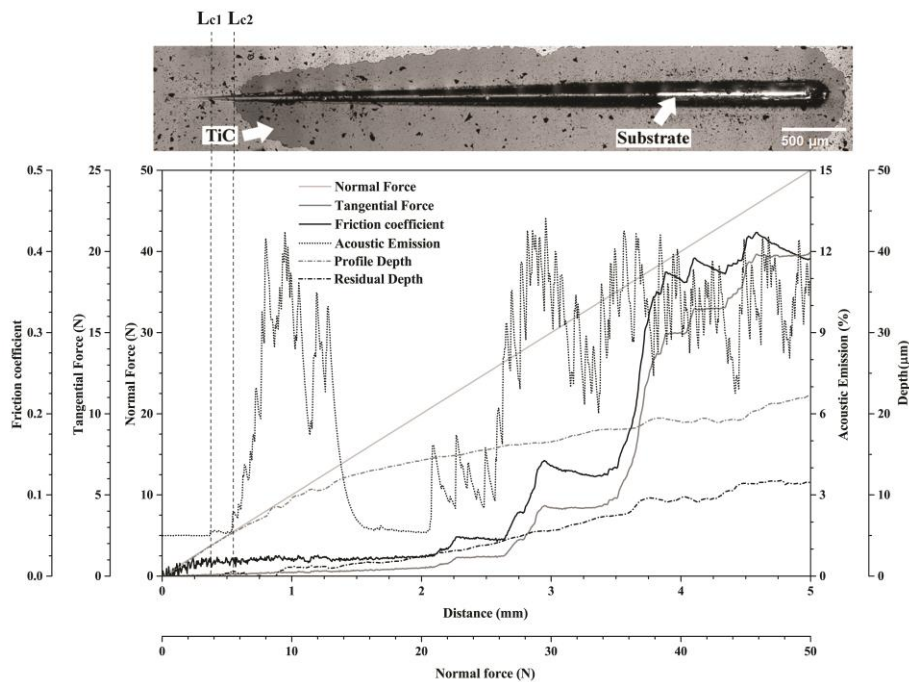
Figure 7 – Scratch test optical image indexed to the graph of monitored responses as a function of the applied normal force and scratch distance of the PEMS+PIID DLC coating.

Accordingly, the three scratch tests per DLC sample were performed and then the resulted mean values of critical loads found for L_{C1} were, 5.3 N and 4.7 N, and for L_{C2}, 14.4 N and 5.4 N, for PIID and PEMS+PIID DLC samples respectively. Moreover, partially magnified images with the cohesive and adhesive damage terms according to ASTM standard atlas are presented on figure 8 for PIID and PEMS+PIID DLC samples.
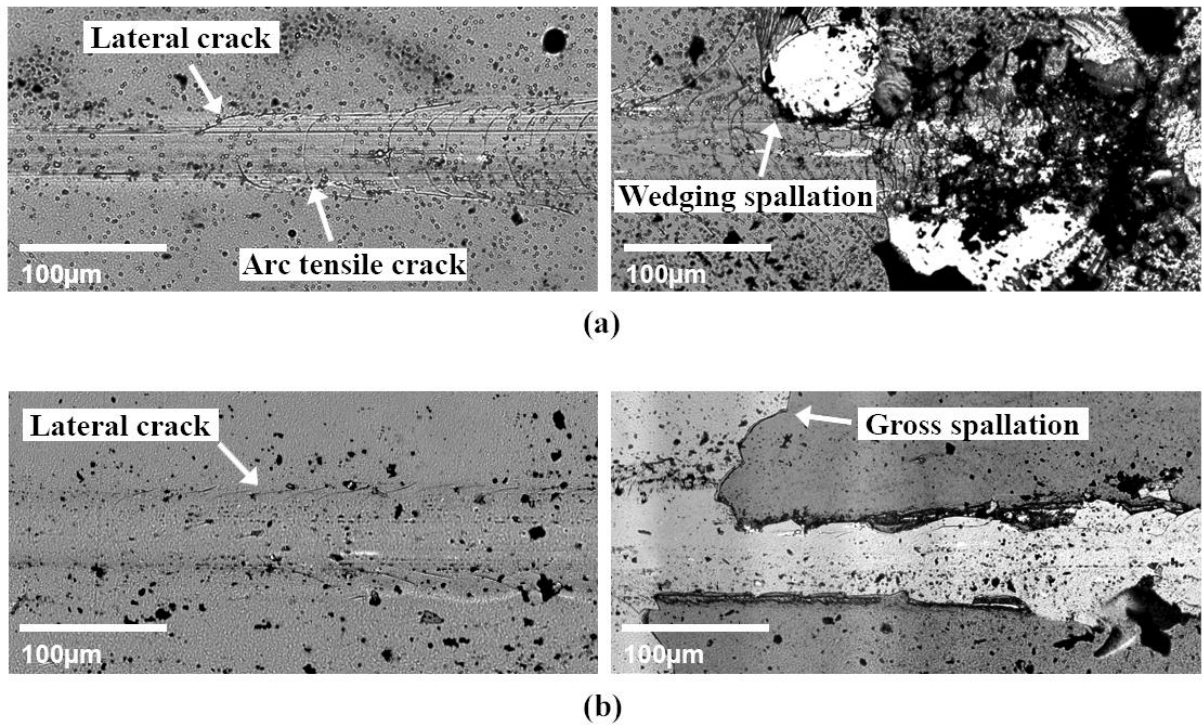
Figure 8 – Partially magnified optical images of the scratch test failures, cohesive at left and adhesive at right, with the identified damage terms of the (a) PIID DLC coating, (b) PEMS+PIID DLC coating.

Both coatings presented sites of lateral tensile cracks as cohesive failures at similar L_{C1} values, however, PIID DLC coating presented also arc tensile cracks inside the trail. The PIID DLC coating adhesive failure was assigned as wedging spallation due to its substrate exposition, regular spacing and "shell" type shape at higher L_{C2} compared to PEMS+PIID coating adhesion failure. Wedging spallation occurs to minimize the amount of elastic energy stored by the compressive stresses produced by the elastic recovery behind the moving indenter during the test and are an also typical brittle failure mode [44]. The gross spallation was identified as PEMS+PIID coating adhesion failure very close to the first lateral cracks appearance which is very common to poorly brittle adhered coatings with high compressive internal stresses. Gross spallation occurs by an extensive crack propagation in a coating interface, in this case between DLC film and TiC interlayer, which provokes a large region delamination as demonstrated [44]. According to ASTM C1624-05 Standard [23], the examination can categorize PIID DLC coating as good interface bonding due only cracking and coating splitting observation and PEMS+PIID DLC coating as a poor interface bonding due to its failure propagation at the interlayer interface. According to Bull and Berasetegui [45], the critical loads measurement can be affected by a number of intrinsic (i.e. scratch test

parameters and equipment) and extrinsic (i.e. coating and substrate properties) factors. As intrinsic parameters and substrate properties were the same for both DLC coated samples, the difference found in the mean values of critical load, especially for L_{C2}, can be associated with the hardness, modulus and residual stress of the coatings. DLC coatings deposited by plasma-base ion implantation are reported to have compressive residual stresses [46] which are associated with the amount of sp3 content on the DLC coating. Therefore, as PIID DLC coating have a lower amount of sp3 bonding content, lower is the compressive residual stress which leads to a minor resistance to traction load behind the indenter resulting in the arc tensile cracking observed inside the trails during coating system stress relaxation. In summary, the enriched sp3 PEMS+PIID DLC coating has improved mechanical properties but also increased the internal compressive stresses, especially in DLC film, leaving this top layer susceptible to large area spallation and poor adhesion that may compromise its use on biomedical applications.

3.6 Tribocorrosion test

Figure 9 shows the OCP measurement before, during and after the tribocorrosion reciprocal sliding tests in 1X PBS solution for the PIID DLC coating, PEMS+PIID DLC coating, and Ti-6Al-4V uncoated samples. All the samples presented corrosion potential of about -440 mV against the Ag/AgCl, NaCl (sat'd) reference electrode during the stabilization period. At the beginning of rubbing, the Ti-6Al-4V uncoated sample presented a large drop on OCP towards cathodic direction while DLC coatings remain same value with some signal noise. This abrupt drop on OCP value of the Ti-6Al-4V uncoated sample occurs due to the depassivation of wear track area. Some positive peaks are observed due to the passivation on the titanium alloy active regions that are constantly removed from alumina sphere during reciprocal sliding movement [47]. The maintenance of OCP average value during rubbing on DLC coatings demonstrated electrochemical stability and successfully mechanical protection to the Ti-6Al-4V substrate. As the movement ceases, small variations of the OCP can be observed on DLC coatings samples with a fast convergence to an average value while the repassivation of the Ti-6Al-4V uncoated are clearly evinced by the curve towards the value of OCP stabilizing period. These results are found in good agreement with other tribocorrison studies on DLC coatings compared to uncoated materials in simulated physiological environments [17,18,48].
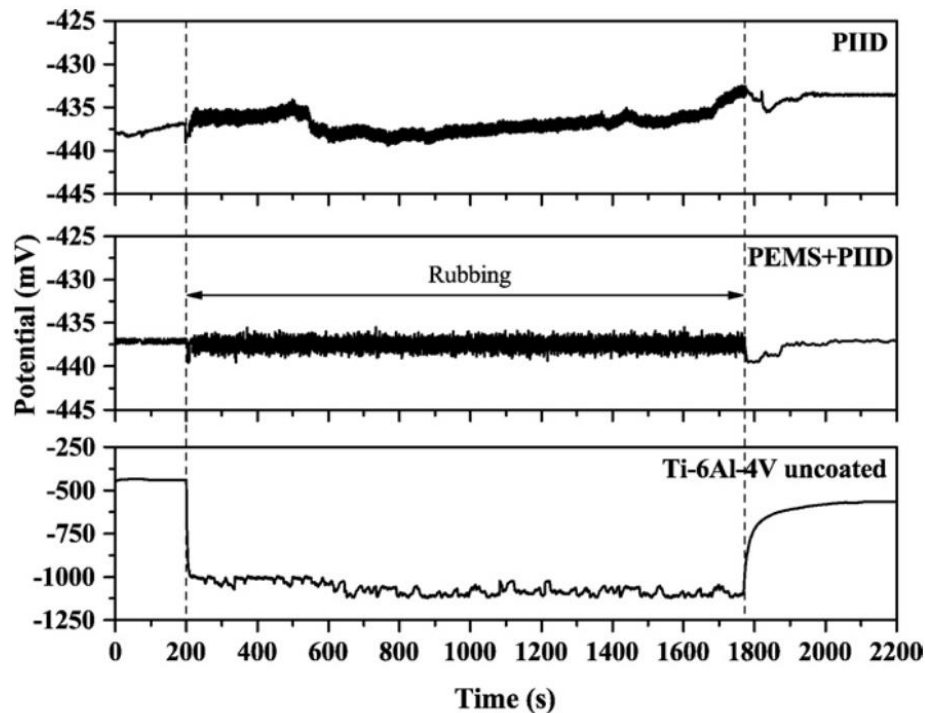
Figure 9 – OCP measurements before, during and after tribocorrosion reciprocal sliding test in 1X PBS solution for the PIID DLC coating, PEMS+PIID DLC coating, and Ti-6Al-4V uncoated samples.

Surface SEM images of the tribocorrosion wear tracks from all the samples are presented in figure 10. No surface failure as cracking or delamination could be observed on both DLC coatings and, besides both exhibited much-smoothed track surfaces, the PIID DLC sample shows more debris amount at the edges of the wear track. Furthermore, the uncoated sample demonstrated clear abrasive grooves inside wear track revealing abrasion as the main wear mechanism on the titanium bare alloy sample. In addition, measured widths of wear tracks were obtained, and the values found were 183.8 µm, 154.1 µm and 971.5 µm for the PIID DLC coating, PEMS+PIID DLC coating, and Ti-6Al-4V uncoated samples respectively. The wear tracks widths revealed a minimum inward movement of the counter-body ball into the coated samples. Therefore, as the contact area between the alumina ball and the DLC coatings are very small, a Hertzian contact stress could be estimated considering a sphere to flat surface contact mode analysis, which results in maximum values greater than 1 GPa. Such value is much higher than the contact pressures found on hip joints during daily activities for example [49,50]. However, as a coating exclusive comparative study the test parameters chosen match the generally used in such tribocorrosion studies.
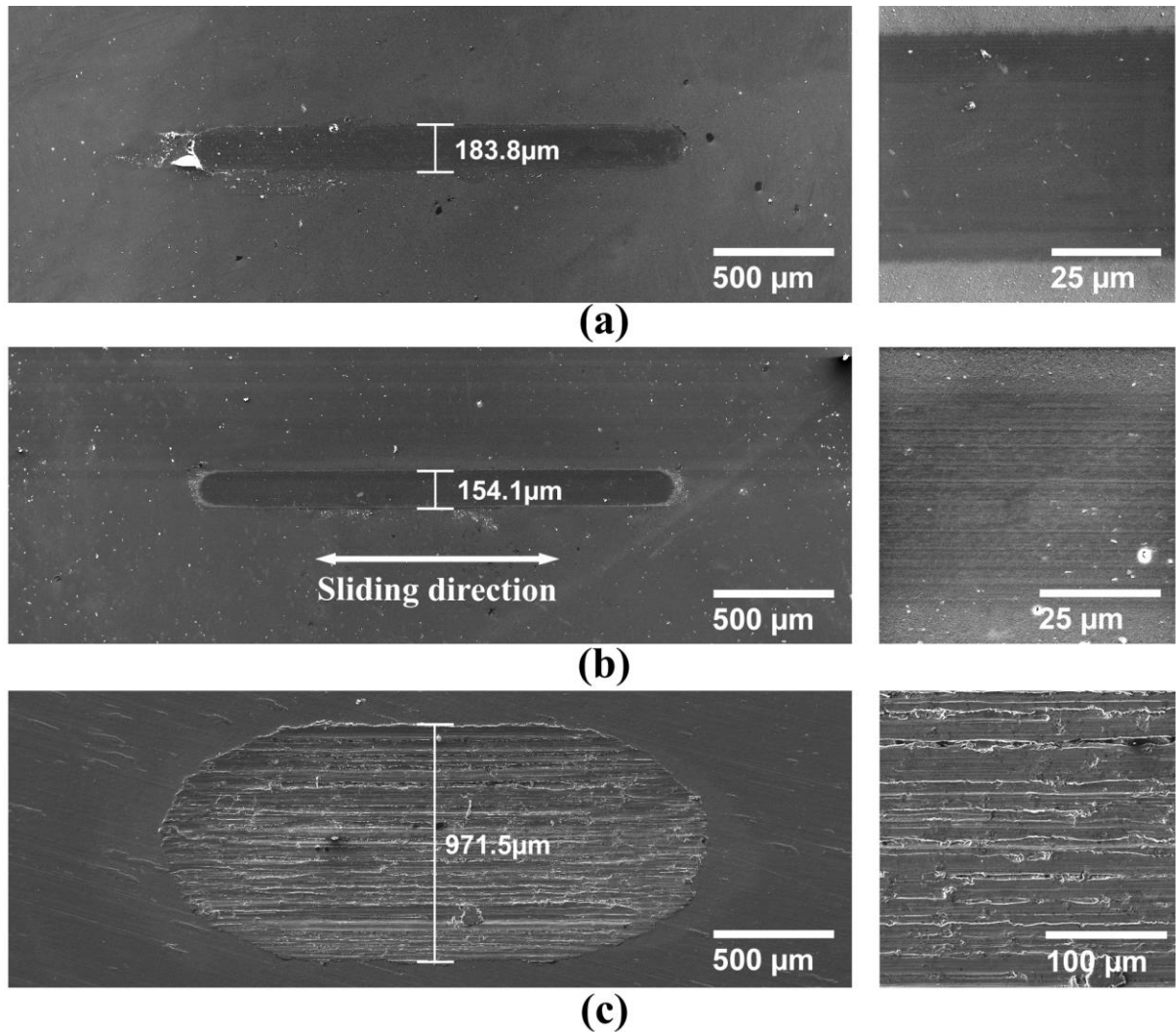
Figure 10 – SEM images of tribocorrosion wear tracks with measured width at left and center track enlarged at right for the (a) PIID DLC coating, (b) PEMS+PIID DLC coating and (c) Ti-6Al-4V uncoated samples.

Figure 11 shows the coefficient of friction (COF) during the tribocorrosion test for the DLC coatings and Ti-6Al-4V uncoated samples. The DLC coatings presented decreasing COF between 0.06 and 0.08 after the running-in regime while Ti-6Al-4V increasing COF from 0.40 to 0.50. The narrow decreasing on DLC coatings COF registered until the end of sliding running distance is attributed to the lubrication of so-called carbon transfer layer originated from the graphitic sites from the coating.
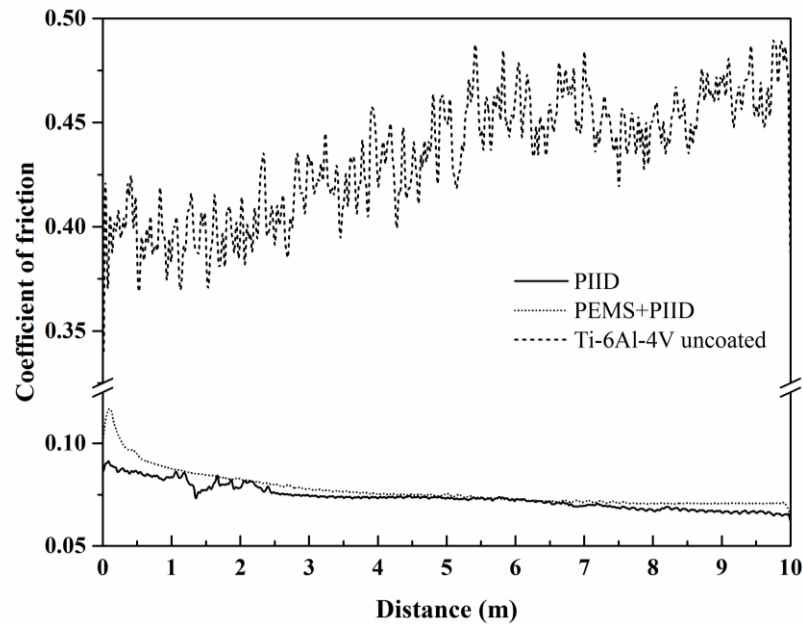
Figure 11 – Coefficient of friction during the tribocorrosion reciprocal sliding test against Al2O3 sphere in 1X PBS solution for the PIID DLC coating, PEMS+PIID DLC coating, and Ti-6Al-4V uncoated samples.

Although the concern of tribocorrosion environment could prevent or disrupt the transfer layer formation and deposition on the tribological pair, carbon adhered to the counter-body ball could be detected with energy-dispersive X-ray spectroscopy (EDS) on the SEM image (figure 12) after the tribocorrosion test on both DLC coatings. Many tribological studies pointed that this transfer layer is responsible to the lower friction coefficient and consequently the good wear behavior of the DLC films against harder materials [8–11]. Besides the presence of carbon adhered on counter body ball, there is no certainty whether this transfer layer is derived simply from the breach of the sp2 bond sites or if occurs a graphitization of the sp3 bond sites, or even both, on the DLC coatings. However, a minor COF value was observed at the initial and the end of the tribocorrosion test on PIID DLC compared PEMS+PIID sample, which suggests that a higher amount of sp2 bond sites can provide faster and iterant contact lubrication between the tribological pair. Moreover, the COF ascending behavior of Ti-6Al-4V uncoated sample relies on the abrasion contribution of the third bodies debris before being taken off the wear track.
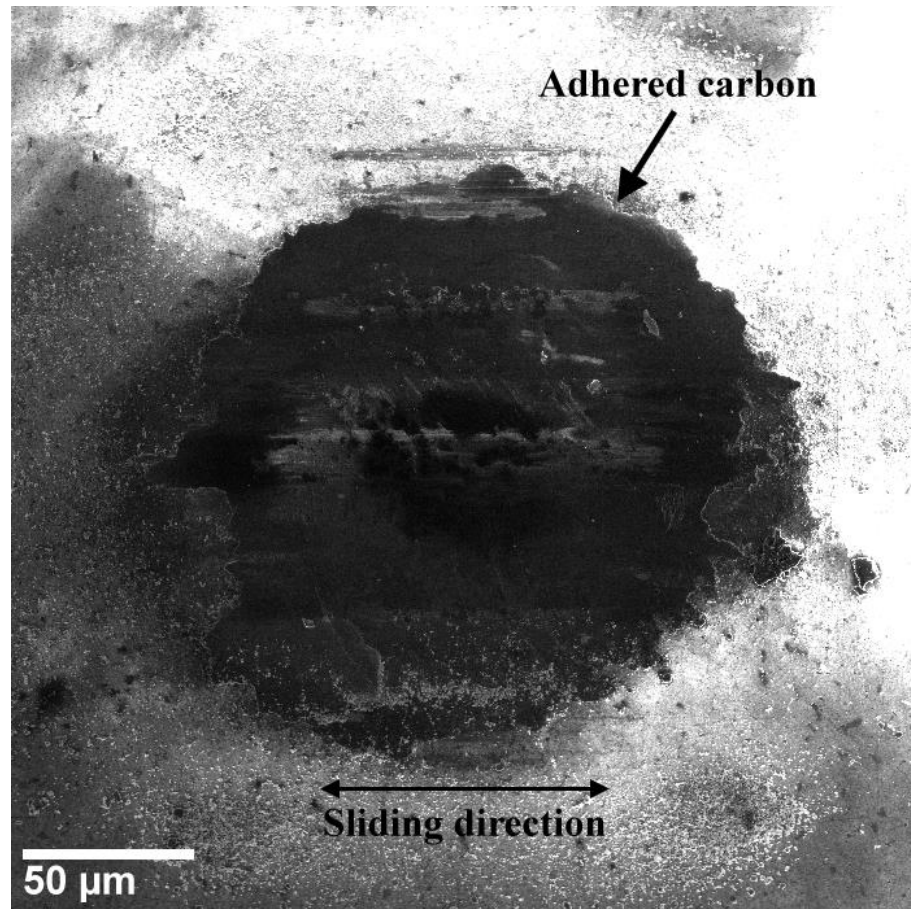
Figure 12 – SEM image of the counter-body alumina ball with adhered carbon after the tribocorrosion test on PEMS+PIID DLC coating sample.

Figure 13 demonstrates the tribocorrosion wear track profiles obtained by a contact profilometer. The PIID DLC coating showed a more rounded wear track profile while PEMS+PIID DLC coating presented a flat bottom inside the profile track. This last resultant profile can be assigned to the improved mechanical properties of DLC layer once COF values are closer between the coated samples.
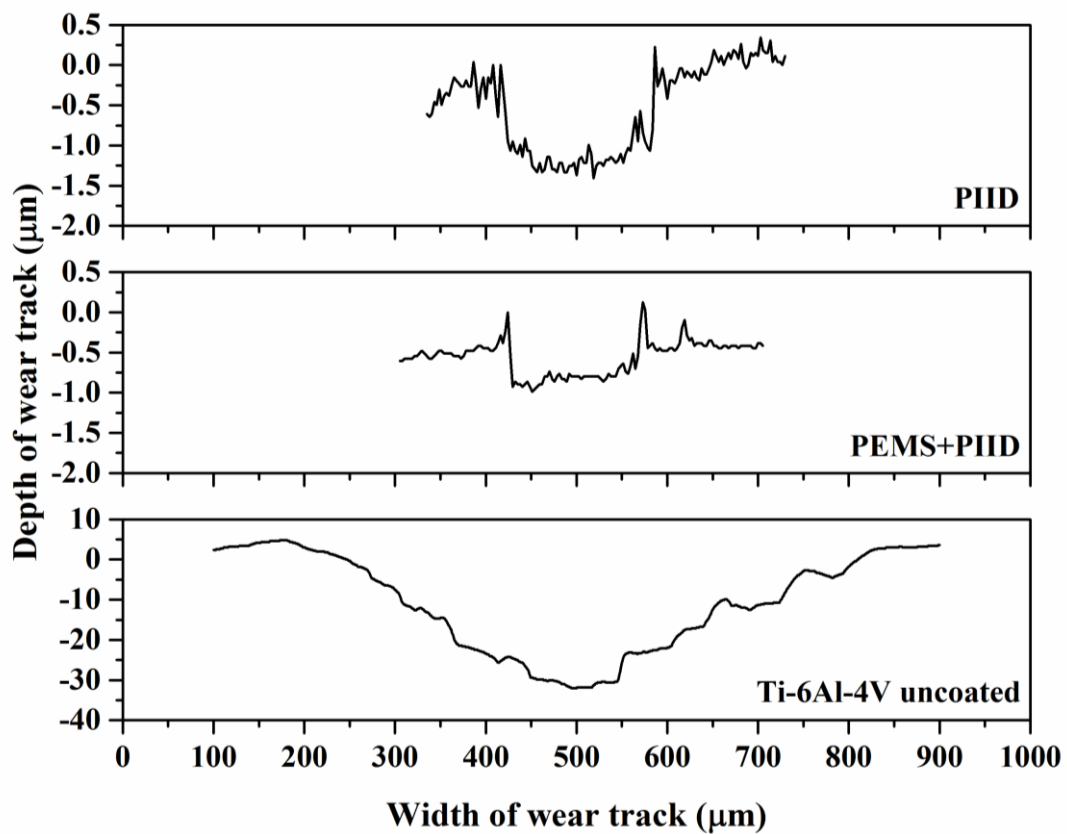
Figure 13 – Wear tracks profiles from the tribocorrosion reciprocal sliding test in 1X PBS solution for the PIID DLC coating, PEMS+PIID DLC coating, and Ti-6Al-4V uncoated samples.

Further, from the profiles of the wear tracks, the loss volumes were obtained and then the resulted samples wear rates are presented in figure 14. As suggested by the small difference between of the elastic strain to failure values, both DLC coating exhibited close wear rate values, however, a statistically significant minor value was obtained on PEMS+PIID DLC coating. This small difference indicates that PEMS+PIID DLC coatings have a preferential sp3/sp2 bonding fraction to optimize the tribocorrosion behavior when compared to PIID DLC coatings. Moreover, in the PIID DLC coatings, the observation of a rounded wear track profile combined with a higher presence of debris justifies the slightly higher wear rate. This proposes that the higher amount of graphitic fraction presents in this coating may accelerate the formation of the carbon transfer layers, but also reveals that these layers are easily removed from the surfaces in contact. In summary, the results have shown that the improved mechanical properties and reduced friction coefficient play together an important role to improve the tribocorrosion behavior on DLC coatings. Hence, an optimal sp3/sp2 bonding fraction was demonstrated to be essential to have an ideal balance between

good mechanical properties and self-solid lubrication capability on these coatings. Finally, the DLC coatings examined presented much lower wear rates and COF compared to usual implant Ti-6Al-4V material under PBS solution and then the DLC coatings have been confirmed as a good option to load-bearing biological applications.
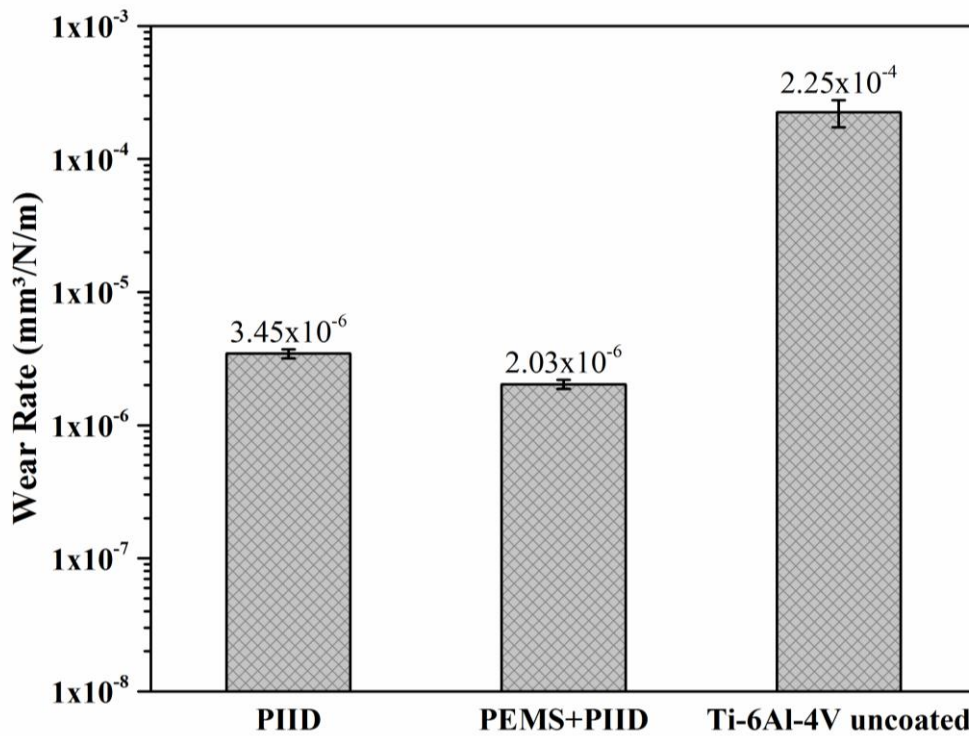
Figure 14 – Wear rate obtained from the loss volume from the tribocorrosion reciprocal sliding test in 1X PBS solution for the PIID DLC coating, PEMS+PIID DLC coating, and Ti-6Al-4V uncoated samples.

4. Conclusions

The tribocorrosion behavior of DLC coatings obtained by plasma enhanced film vapor depositions techniques under simulated physiological fluid was studied. Both DLC coatings presented at least 5 times less friction coefficient and less than 2% of wear rate of the usual implant Ti-6Al-4V alloy under the test conditions. Moreover, the findings between the DLC coatings obtained by PIID and PEMS+PIID techniques indicate that the tribocorrosion behavior is associated with the mechanical properties and the carbon transfer layer formation, which in turn is strongly related to the fraction of sp2 and sp3 bonds presents on its structure. Although the recurrent carbon transfer layer diminishes the coefficient of friction along the reciprocal sliding test under PBS, it also inflicted negatively on the wear rate due to its poor shear resistance. Furthermore, the elastic strain to failure presented a good correlation to the

wear rate obtained for the DLC coatings. The importance to have a proper sp2/sp3 bond fraction to achieve optimal tribocorrosion behavior on DLC coatings was demonstrated. This favorable condition was verified on the DLC deposited by the advanced plasma enhanced techniques and therefore, the PIID and PEMS+PIID deposition systems proposed are very promissory to achieve an improved tribocorrosion behavior in DLC-Coated Ti-6Al-4V alloy implants.

Acknowledgments

References

[1]   C. Gwam, J.B. Mistry, N. Mohamed, M. Thomas, K.C. Bigart, M.A. Mont, R.E. Delanois, Current Epidemiology of Revision Total Hip Arthroplasty in the United States: National Inpatient Sample 2009 to 2013, J. Arthroplasty. (2017). doi:10.1016/j.arth.2017.02.046.

[2]   M. Sundfeldt, L. V Carlsson, C.B. Johansson, P. Thomsen, C. Gretzer, Aseptic loosening, not only a question of wear: a review of different theories., Acta Orthop. 77 (2006) 177–97. doi:10.1080/17453670610045902.

[3]   S. Kurtz, F. Mowat, K. Ong, N. Chan, E. Lau, M. Halpern, Prevalence of Primary and Revision Total Hip and Knee Arthroplasty in the United States From 1990 Through 2002, Jounal Bone Jt. Surg. 87–A (2005) 1487–1497. doi:10.2106/JBJS.D.02441.

[4]   Z. Paszenda, W. Walke, S. Jadacka, Electrochemical investigations of Ti6Al4V and Ti6Al7Nb alloys used on implants in bone surgery, J. Achiev. Mater. Manuf. Eng. 38 (2010) 24–32.

[5]   V.S.A. Challa, S. Mali, R.D.K. Misra, Reduced toxicity and superior cellular response of preosteoblasts to Ti-6Al-7Nb alloy and comparison with Ti-6Al-4V, J. Biomed. Mater. Res. - Part A. 101 A (2013) 2083–2089. doi:10.1002/jbm.a.34492.

[6]   J. Robertson, Diamond-like amorphous carbon, Mater. Sci. Eng. R Reports. 37 (2002) 129–281. doi:10.1016/S0927-796X(02)00005-0.

[7]   A. Grill, Diamond-like carbon: state of the art, Diam. Relat. Mater. 8 (1999) 428–434. doi:10.1016/S0925-9635(98)00262-3.

[8]   R. Hauert, A review of modified DLC coatings for biological applications, Diam. Relat. Mater. 12 (2003) 583–589. doi:10.1016/S0925-9635(03)00081-5.

[9]   A. Grill, Review of the tribology of diamond-like carbon, Wear. 168 (1993) 143–153. doi:10.1016/0043-1648(93)90210-D.

[10]   Y. Liu, A. Erdemir, E.I. Meletis, A study of the wear mechanism of diamond-like carbon films 1, Surf. Coatings Technol. 82 (1996) 48–56. doi:10.1016/0257-8972(95)02623-1.

[11]   A. Erdemir, C. Bindal, G.R. Fenske, C. Zuiker, P. Wilbur, Characterization of transfer layers forming on surfaces sliding against diamond-like carbon, Surf. Coatings Technol. 86–87 (1996) 692–697. doi:10.1016/S0257-8972(96)03073-3.

[12]   T.T. Liao, T.F. Zhang, S.S. Li, Q.Y. Deng, B.J. Wu, Y.Z. Zhang, Y.J. Zhou, Y.B. Guo, Y.X. Leng, N. Huang, Biological responses of diamond-like carbon (DLC) films with different structures in biomedical application, Mater. Sci. Eng. C. 69 (2016) 751–759. doi:10.1016/j.msec.2016.07.064.

[13]   M. Azzi, P. Amirault, M. Paquette, J.E. Klemberg-Sapieha, L. Martinu, Corrosion performance and mechanical stability of 316L/DLC coating system: Role of interlayers, Surf. Coatings Technol. 204 (2010) 3986–3994. doi:10.1016/j.surfcoat.2010.05.004.

[14]   K.W. Chen, J.F. Lin, The study of adhesion and nanomechanical properties of DLC films deposited on tool steels, Thin Solid Films. 517 (2009) 4916–4920. doi:10.1016/j.tsf.2009.03.124.

[15]   J. Lin, W.D. Sproul, R. Wei, R. Chistyakov, Diamond like carbon films deposited by HiPIMS using oscillatory voltage pulses, Surf. Coatings Technol. 258 (2014) 1212–1222. doi:10.1016/j.surfcoat.2014.06.061.

[16]   S.J. Bull, Tribology of carbon coatings: DLC, diamond and beyond, Diam. Relat. Mater. 4 (1995) 827–836. doi:10.1016/0925-9635(94)05325-1.

[17]   T.M. Manhabosco, I.L. Müller, Tribocorrosion of diamond-like carbon deposited on Ti6Al4V, Tribol. Lett. 33 (2009) 193–197. doi:10.1007/s11249-009-9408-8.

[18]   G.H. Zhao, R.E. Aune, N. Espallargas, Tribocorrosion studies of metallic biomaterials: The effect of plasma nitriding and DLC surface modifications, J. Mech. Behav. Biomed. Mater. 63 (2016) 100–114. doi:10.1016/j.jmbbm.2016.06.014.

[19]   Y. Oka, M. Nishijima, K. Hiraga, M. Yatsuzuka, Effect of ion implantation layer on adhesion of DLC film by plasma-based ion implantation and deposition, Surf. Coatings Technol. 201 (2007) 6647–6650. doi:10.1016/j.surfcoat.2006.09.027.

[20]   R. Wei, Development of new technologies and practical applications of plasma immersion ion deposition (PIID), Surf. Coatings Technol. 204 (2010) 2869–2874. doi:10.1016/j.surfcoat.2010.01.046.

[21]   N.A. Sánchez, C. Rincón, G. Zambrano, H. Galindo, P. Prieto, Characterization of diamond-like carbon (DLC) thin films prepared by r.f. magnetron sputtering, Thin Solid Films. 373 (2000) 247–250. doi:10.1016/S0040-6090(00)01090-7.

[22]   R. Wei, E. Langa, C. Rincon, J.H. Arps, Deposition of thick nitrides and carbonitrides

for sand erosion protection, Surf. Coatings Technol. 201 (2006) 4453–4459. doi:10.1016/j.surfcoat.2006.08.091.

[23]   ASTM, Standard Test Method for Adhesion Strength and Mechanical Failure Modes of, 5 (2013) 1–29. doi:10.1520/C1624-05R10.Scope.

[24]   J. Lin, X. Zhang, P. Lee, R. Wei, Thick diamond like carbon coatings deposited by deep oscillation magnetron sputtering, Surf. Coatings Technol. 315 (2017) 294–302. doi:10.1016/j.surfcoat.2017.02.044.

[25]   Q. Wang, F. Zhou, Z. Zhou, Y. Yang, C. Yan, C. Wang, W. Zhang, L.K.Y. Li, I. Bello, S.T. Lee, Influence of carbon content on the microstructure and tribological properties of TiN(C) coatings in water lubrication, Surf. Coatings Technol. 206 (2012) 3777–3787. doi:10.1016/j.surfcoat.2012.03.041.

[26]   R.W. A.M. Abd El-Rahman, A comparative study of conventional magnetron sputter deposited and plasma enhanced magnetron sputter deposited Ti–Si–C–N nanocomposite coatings, Surf. Coatings Technol. 241 (2014) 74–79. doi:10.1016/j.surfcoat.2013.08.049.

[27]   R. Wei, C. Rincon, E. Langa, Q. Yang, Microstructure and tribological performance of nanocomposite Ti–Si–C–N coatings deposited using hexamethyldisilazane precursor, J. Vac. Sci. Technol. A Vacuum, Surfaces, Film. 28 (2010) 1126. doi:10.1116/1.3463709.

[28]   a. M. Abd El-Rahman, R. Wei, Effect of ion bombardment on structural, mechanical, erosion and corrosion properties of Ti–Si–C–N nanocomposite coatings, Surf. Coatings Technol. 258 (2014) 320–328. doi:10.1016/j.surfcoat.2014.09.006.

[29]   V.N. Apakina, A.L. Karuzskii, M.S. Kogan, A.V. Kvit, N.N. Melnik, Y.A. Mityagin, V.N. Murzin, A.A. Orlikovsky, A.V. Perestoronin, S.D. Tkachenko, N.A. Volchkov, Studies of nanoscale structure and its transformation in pulsed-laser deposited dense diamond-like carbon films, Diam. Relat. Mater. 6 (1997) 564–568. doi:10.1016/S0925-9635(96)00629-2.

[30]   S.P. Bugaev, K. V. Oskomov, V.G. Podkovyrov, S. V. Smaykina, N.S. Sochugov, Use of the hydrocarbon plasma of a low-pressure arc discharge for deposition of highly adhesive a-C:H films, Surf. Coatings Technol. 135 (2000) 18–26. doi:10.1016/S0257-8972(00)00919-1.

[31]   F.C. Tai, S.C. Lee, J. Chen, C. Wei, S.H. Chang, Multipeak fitting analysis of Raman spectra on DLCH film, J. Raman Spectrosc. 40 (2009) 1055–1059. doi:10.1002/jrs.2234.

[32]   a. Ferrari, J. Robertson, Interpretation of Raman spectra of disordered and amorphous carbon, Phys. Rev. B. 61 (2000) 14095–14107. doi:10.1103/PhysRevB.61.14095.

[33]   J. Yang, C. Shim, D. Jung, Plasma enhanced CVD of low dielectric constant plasma polymerized decahydronaphthalene thin films, Chem. Vap. Depos. 8 (2002) 35–37. doi:10.1002/1521-3862(20020116)8:1<35::AID-CVDE35>3.0.CO;2-B.

[34]   T.Y. Leung, W.F. Man, P.K. Lim, W.C. Chan, F. Gaspari, Determination of the sp 3 / sp 2 ratio of a-C : H by XPS and XAES, 254 (1999) 156–160.

[35] J. Wang, J. Ma, W. Huang, L. Wang, H. He, C. Liu, The investigation of the structures and tribological properties of F-DLC coatings deposited on Ti-6Al-4V alloys, Surf. Coatings Technol. 316 (2017) 22–29. doi:10.1016/j.surfcoat.2017.02.065.

[36] X.B. Yan, T. Xu, S.R. Yang, H.W. Liu, Q.J. Xue, Characterization of hydrogenated diamond-like carbon films electrochemically deposited on a silicon substrate, J. Phys. D. Appl. Phys. 37 (2004) 2416–2424. doi:10.1088/0022-3727/37/17/012.

[37] J. Filik, P.W. May, S.R.J. Pearce, R.K. Wild, K.R. Hallam, XPS and laser Raman analysis of hydrogenated amorphous carbon films, Diam. Relat. Mater. 12 (2003) 974–978. doi:10.1016/S0925-9635(02)00374-6.

[38] E.T. Uzumaki, C.S. Lambert, W.D. Belangero, C.M.A. Freire, C.A.C. Zavaglia, Evaluation of diamond-like carbon coatings produced by plasma immersion for orthopaedic applications, Diam. Relat. Mater. 15 (2006) 982–988. doi:10.1016/j.diamond.2005.12.006.

[39] Y. Zheng, D. Liu, X. Liu, L. Li, Ti--TiC--TiC/DLC gradient nano-composite film on a biomedical NiTi alloy, Biomed. Mater. 3 (2008) 44103–6. doi:10.1088/1748-6041/3/4/044103.

[40] A. Leyland, A. Matthews, On the significance of the H/E ratio in wear control: A nanocomposite coating approach to optimised tribological behaviour, Wear. 246 (2000) 1–11. doi:10.1016/S0043-1648(00)00488-9.

[41] A. Leyland, A. Matthews, Design criteria for wear-resistant nanostructured and glassy-metal coatings, Surf. Coatings Technol. 177–178 (2004) 317–324. doi:10.1016/j.surfcoat.2003.09.011.

[42] J. Musil, F. Kunc, H. Zeman, H. Poláková, Relationships between hardness, Young's modulus and elastic recovery in hard nanocomposite coatings, Surf. Coatings Technol. 154 (2002) 304–313. doi:10.1016/S0257-8972(01)01714-5.

[43] H. Zaidi, A. Djamai, K.J. Chin, T. Mathia, Characterisation of DLC coating adherence by scratch testing, Tribol. Int. 39 (2006) 124–128. doi:10.1016/j.triboint.2005.04.016.

[44] S.J. Bull, Failure modes in scratch adhesion testing, Surf. Coatings Technol. 50 (1991) 25–32. doi:10.1016/0257-8972(91)90188-3.

[45] S.J. Bull, E. G.-Berasetegui E., An overview of the potential of quantitative coating adhesion measurement by scratch testing, Tribol. Interface Eng. Ser. 51 (2006) 136–165. doi:10.1016/S0167-8922(06)80043-X.

[46] Y. Oka, M. Kirinuki, Y. Nishimura, K. Azuma, E. Fujiwara, M. Yatsuzuka, Measurement of residual stress in DLC films prepared by plasma-based ion implantation and deposition, Surf. Coatings Technol. 186 (2004) 141–145. doi:10.1016/j.surfcoat.2004.04.010.

[47] J.C.M. de Souza, Biotribocorrosion behavior of titanium in simulated oral environments, J. Chem. Inf. Model. 53 (2009) 1689–1699. doi:10.1017/CBO9781107415324.004.

[48]   J. Liu, X. Wang, B.J. Wu, T.F. Zhang, Y.X. Leng, N. Huang, Tribocorrosion behavior of DLC-coated CoCrMo alloy in simulated biological environment, Vacuum. 92 (2013) 39–43. doi:10.1016/j.vacuum.2012.11.017.

[49]   H. Yoshida, A. Faust, J. Wilckens, M. Kitagawa, J. Fetto, E.Y.S. Chao, Three-dimensional dynamic hip contact area and pressure distribution during activities of daily living, J. Biomech. 39 (2006) 1996–2004. doi:10.1016/j.jbiomech.2005.06.026.

[50]   W.A. Hodge, W.H. Harris, Contact pressures in the human hip joint measured in vivo, 83 (1986) 2879–2883.

4 **ARTIGO 2**

Tribocorrosion Behavior of Low Friction TiSiCN Nanocomposite Coatings Deposited on Titanium Alloy for Biomedical Applications

Andre Hatem[a], Jianliang Lin[b], Ronghua Wei[b], Ricardo D. Torres[a], Carlos Laurindo[a], Gelson Biscaia de Souza[c], Paulo Soares[a*]

[a] Department of Mechanical Engineering, Polytechnic School, Pontifícia Universidade Católica do Paraná, Curitiba, PR, 80215-901, Brazil.
[b] Surface Engineering & Materials Chemistry, Materials Engineering Department, Southwest Research Institute, San Antonio, TX, 78238, USA.
[c] Physics Department, Universidade Estadual de Ponta Grossa, Ponta Grossa, PR, 84030-900, Brazil.

Corresponding author
Paulo Soares, Prof. Dr.
Pontifícia Universidade Católica do Paraná
Polytechnic School - Mechanical Engineering Department
Rua Imaculada Conceição, 1155 – Prado Velho
ParqTec – Bl. 9
80215-901 Curitiba, PR – Brasil
+55 (41) 3271-1338
pa.soares@pucpr.br

Abstract

The quaternary Ti-Si-C-N nanocomposite is regarded to be promising one in the biomedical field due to its improved tribocorrosion performance and biocompatibility. The deposition of such material on biomedical components surfaces can extend its lifespan by minimizing wear debris and ion releasing inside the physiological environment. Therefore, this work investigates the tribocorrosion behavior of low friction Ti-Si-C-N nanocomposite coatings applied on the ASTM F136 titanium alloy immersed in a phosphate-buffered solution (PBS). The coatings were obtained by the plasma-enhanced magnetron sputtering (PEMS) technique using an assorted precursor flow range of tetramethylsilane (TMS) and hexamethyldisilazane (HMDSN) liquid along with acetylene (C2H2) gas. Reciprocal sliding tribocorrosion tests were performed under PBS solution on the samples and compared to a Ti-6Al-4V bare alloy sample. The microstructure, morphology, chemical structure, mechanical properties, and adhesion of the coated samples were also evaluated. The results presented an expressive reduction of at least 97% in the wear rate of the low friction Ti-(Si)-C-N nanocomposite coatings compared to the titanium bare alloy sample. The tribocorrosion performance of the coated samples demonstrated a strong correlation within the Silicon and Carbon content presented on coatings chemical compositions. As consequence, the roles of nanocrystallites refinement, the presence of amorphous carbon region and the oxides generation were demonstrated as relevant characteristics to improve the tribocorrosion behavior of Ti-Si-C-N nanocomposite.

Keywords: Titanium alloy, TiSiCN coatings, XRD, XPS, SEM, Adhesion, Hardness, Tribocorrosion

1. Introduction

The promotion of superior tribocorrosion performance in titanium alloy prosthesis remains as a crucial goal in the failure prevention of long-term applications. The mechanism of tribocorrosion accelerates the degradation of the implant material within the biomedical body resulting in a broad generation of particulate wear debris in the prosthesis interface with surrounding tissue [1–4]. The biological response to wear debris may induce inflammatory reactions, bone resorption, hypersensitivity diseases and osteolysis [5,6]. These conditions often result in poor fixation of the prosthesis components requiring a revision arthroplasty after 15 to 20 years of placement procedure [7,8]. In fact, the aseptic loosening has been confirmed as the principal diagnostic for revision surgery in total hip, knee and ankle arthroplasties [9–11]. Additionally, the tribocorrosion process favors an undesirable amount of ion dissolution from the alloying elements presented in the implant material composition, such as Aluminum and Vanadium in case of the usual titanium ASTM F136 alloy [12]. For instance, high ion concentrations of these elements in the blood may cause some adverse reactions as cytotoxic effects and neurological disorders in the patients [6,13,14]. Since the prevention of the tribocorrosion initiation events, as load bearing and micromovements conditions is practically unfeasible in implants, a reduction of the friction coefficient in the exertive interface has been indicated as one of the effective approaches to diminish the wear and corrosion products [15]. In recent years, several reports demonstrated the deposition of thin Diamond-like carbon (DLC) films as a good alternative to enhance the tribocorrosion behavior of titanium alloy surfaces in the biomedical environment [16–20]. In addition to the improvement in the mechanical properties and corrosion resistance, the wear rate reduction verified on the tribocorrosion tests of DLC-coated surfaces is attributed to the formation of a carbon transfer layer on the tribo-pair which acts as a solid lubricant and hence, drastically lowers the coefficient of friction [21–23]. However, the low adhesion strength limits its application on the biomedical field. High residual stresses introduced during the film deposition can cause extensive delamination in DLC-coated materials under critical loads [24]. Other low friction coatings have been also proposed to protect the prosthesis components, such as the silicon carbide (SiC), the titanium nitride (TiN), the titanium diboride (TiB_2), the titanium carbonitride (TiCN), the titanium aluminum nitride (TiAlN), the chromium nitride (CrN), the chromium carbonitride (CrCN) and the titanium silicon carbonitride (TiSiCN) [25]. Same as this last, others nanocomposites thin films based on quaternary transition metal nitride systems have demonstrated improved wear and/or corrosion resistance in comparison to the less complex systems (binary and ternary), as the

TiNbSiN [26], TiAlSiN [27] and TiCrSiN [28]. Therefore, low friction biocompatible quaternary coatings, if well adhered to the titanium substrate, may represent a solution to attend the demand for an extended lifespan of titanium alloy implants, by enhancing its tribocorrosion behavior in the biomedical environment.

In the search for new low friction biocompatible coatings, the quaternary Ti-Si-C-N nanocomposite is regarded to be promising one in the biomedical field. This titanium-based coating has been recommended for applications that require high wear resistance combined with a low friction due to its reported enhanced mechanical properties, good toughness and self-lubricious behavior [29–34]. The superior properties verified on the low friction Ti-Si-C-N nanocomposite coatings are often associated to an optimized structure composed by nanosized crystallites of Ti(C, N) embedded in an amorphous matrix of Si_3N_4/SiC with segregated regions of amorphous carbon (a-C) [35–37]. The strengthening mechanism on such structure is based on the TiN/Si_3N_4 model system proposed by Veprek et al. [38]. However, a recent work [39] suggested the phases of Si_3N_4, C, and CN_x in a crystallized form along with the Ti(C, N) nanocrystals to comprise the nanocomposite structure, in which the strengthening effect would be given by a coherent-interface mechanism. Such presented phases are often evaluated by X-ray diffraction (XRD) and X-ray photoelectron spectroscopy (XPS) characterization techniques on these coatings [30,36,40,41]. Apart from the enhanced properties, the Ti-Si-C-N nanocomposite coatings have demonstrated good tribocorrosion performance. Wang et al. [42] have investigated the tribocorrosion behavior of Ti-Si-C-N coatings obtained by arc ion plating with different carbon contents under artificial seawater. The authors verified low wearing rates associated with the formation of a lubricious graphite layer and a maximized hardness at an optimum value of carbon content. Indeed, carbon and silicon elements are pointed as grain refiners on Ti-Si-C-N nanocomposite structure [37,43]. In addition, the deposition techniques employed in the synthesis of the Ti-Si-C-N coatings demonstrated a strong influence on the mechanical and tribological properties. As a case, high ratios of H/E (elastic strain to failure) and H^3/E^2 (resistance to plastic deformation) have been achieved in Ti-Si-C-N coatings obtained by plasma enhanced magnetron sputtering (PEMS) compared to the conventional magnetron sputtering (CMS) technique [44]. Finally, similar hard coating compositions, such as the Ti-Si-C-N-O, presented low cytotoxicity, especially for low values of C/Si and N/Ti fractions [45]. Therefore, the low friction Ti-Si-C-N coatings have confirmed desirable characteristics to achieve an improved lifetime in biomedical applications. Still, few are the studies published on the tribocorrosion behavior of such nanocomposite coatings.

Accordingly, this work aims to investigate the tribocorrosion behavior of low friction Ti-Si-C-N nanocomposite coatings applied on a biomedical titanium alloy immersed in phosphate-buffered saline (PBS). The coatings were obtained by the plasma-enhanced magnetron sputtering (PEMS) technique using an assorted flow range from 0 to 9 sccm (standard cubic centimeters per minute) of tetramethylsilane (TMS) along with acetylene (C_2H_2) gas precursors. These conditions were applied to verify the tribocorrosion performance from coatings with distinct elemental compositions. Also, an alternative condition with hexamethyldisilazane (HMDSN) liquid precursor instead of TMS was included in this study. The HMDSN precursor has been proven to be safer for handling and also to produce Ti-Si-C-N coatings with much lower coefficients of friction over the coatings obtained by TMS precursor [29]. The evaluation of coatings microstructure, morphology, chemical structure, mechanical properties, and adhesion will also be presented.

2. Experimental Procedure

2.1 Coating depositions

Titanium alloy samples were obtained from a Ti-6Al-4V ELI (ASTM F136) annealed bar with 25.4 mm diameter x 2 mm thick discs by electrical discharge cutting. The samples were prepared by grinding with SiC paper ranging from 320 to 1200 grit sizes and then polishing using colloidal silica (0.04 µm). The Ti-(Si)-C-N coatings were deposited by sputtering two Ti metal targets (with 15.2 cm diameter) in a reactive atmosphere using a so-called plasma enhanced magnetron sputtering (PEMS) process by the Southwest Research Institute (SwRI) deposition system [46]. The PEMS technique is an advanced version of conventional magnetron sputtering, which introduces a global plasma that is generated by an electron source or other means such as RF excitation to enhance the ionization of the plasma [31]. Prior to all depositions, the chamber was heated to 200 °C and pumped down to a base pressure below $3x10^{-4}$ Pa. A Ti/TiN bond layer was deposited to enhance the adhesion strength of all coatings. Then TiSiCN coatings with thicknesses in the range of 8-10 µm were deposited. The Ti targets were powered by continuous dc magnetron sputtering (dcMS) at a 4 kW average target power each (MDX, 10kW, Advanced Energy, Inc). The working pressure was 0.4 Pa. A dc bias voltage of -60 V was used for all coating depositions. The reactive mixture with flow rates of 190 sccm of argon gas (Ar), 45 sccm of nitrogen gas (N_2) and 30 sccm acetylene gas (C_2H_2) was utilized within a Silicon precursor. Two Silicon precursors were used to obtain the TiSiCN coatings, the trimethylsilane gas ((CH_3)$_3$SiH, TMS) and the

hexamethyldisilazane liquid ((CH_3)$_6$$Si_2$NH, HMDSN). The flow rates selected for the TMS were 0, 1.5, 3, 6 and 9 sccm, while for the HMDSN was maintained at 3 g/h.

2.2 Coatings characterization

The surface morphologies and cross-sectional microstructures of the Ti-(Si)-C-N nanocomposite coatings were obtained by scanning electron microscopy (SEM) (TESCAN, VEGA 3 LM) in secondary electrons detection mode at 20 kV. The coatings chemical composition were obtained by energy dispersive spectroscopy (EDS). The average surface roughness (Ra) of each coated sample was determined by five measurements for cut-off (lr) of 0.08 mm using a contact profilometer (Taylor Hobson, Talysurf Series 2) with a resolution of 12 nm and accuracy of up to 0.006 µm. The structural characterization was assessed by Thin film X-ray diffraction (TF-XRD) using a Shimadzu XRD-7000 with CuKα radiation (λ=1.540600 Å) operated at 30 kV and 40 mA. The scanning angle ranged from 10° to 100° at a scanning speed of 1°/min with 0.02° step size, at an angle of incidence of 2.5° in thin film mode. Then, nanocrystallites size were estimated by the Scherrer equation [47,48] at the full width at half-maximum value from the predominant peak adjusted by a Gaussian fitting curve. X-ray photoelectron spectroscopy (XPS, Scienta Omicron ESCA spectrometer) was performed using a monochromatic AlKα X-ray source (1486.7 eV). Survey spectra were collected from 0 to 1200 eV, and high-resolution spectra were collected for C1s, Ti2p, Si2p, and N1s peaks. All spectra were referenced by setting the C 1s peak to 284.8 eV. The peak areas were quantified using a Gaussian-Lorentzian fitting procedure after performing Shirley background subtraction.

Further, hardness and elastic modulus of the coatings were assessed by means of nanoindentation using an ASMEC universal nanomechanical tester (UNAT) with 20 mN force resolution in quasi-continuous stiffness measurements (QCSM) mode with a Berkovich diamond tip. The indentations were set in three columns with three indentations each, the indentations were 75 µm equally spaced, with the applied maximum load of 400 mN. Then, the mean values and standard deviations for the hardness and elastic modulus were obtained from the indentations performed in each sample. The H/E and H^3/E^2 ratios were determined taking into account the mean hardness and elastic modulus between the values acquired along the coatings depth. The adhesion strength of the coatings was verified by scratch test (CSM Instruments RSX-S-BE-0000) following the ASTM C1624-95 standard [49]. Three linear progressive load scratch tests were performed on each sample using standard parameter values of 100 N/min loading rate, 10 mm/min horizontal displacement rate, in a total scratch

length of 5 mm, resulting in final test load of 50 N. Then, the two-level critical scratch loads (Lc1 and Lc2) were assigned at the normal load at the beginning of cohesive and adhesion failures. The failures were identified using optical microscope images of the scratches along with the acoustic emission and stylus tangential force signals data collected during the tests. Also, each failure was classified according to the scratch atlas presented in the ASTM C1624-05 standard [49]. The presented critical scratch loads and its errors were obtained by the mean values and standard deviation of the scratch tests performed on each sample. Finally, tribocorrosion tests were conducted under phosphate-buffered saline (PBS) solution at 1x concentration (137 mM NaCl, 2.7 mM KCl, 10 mM Na_2HPO_4, 1 mM KH_2PO_4, pH 7.4). The electrolyte cell was set-up in a three-electrode system in which the Ti-(Si)-C-N coated samples, Ag/AgCl, NaCl (sat'd) electrode, and Pt wire electrode were used as the working, reference and counter electrodes, respectively. The coated surface of the samples were painted, leaving an active area of 0.36 cm² exposed to the electrolyte solution. The open circuit potentials (OCP) were monitored by a potentiostat (Ivium) during the entire test. Firstly, the samples were plunged in a vat with 700 ml of PBS for 1 hour to stabilize the OCP. Then, using a universal tribometer (Anton-Paar) equipment, reciprocal sliding tests were performed with 2 mm amplitude at the maximum linear speed of 1 cm/s, applying a 10 N normal force and using a 6 mm diameter Al_2O_3 ball in a 10 meters total distance. At the rubbing ceasing, the samples were kept for more 30 minutes in the solution to allow any repassivation. Images of the wear tracks morphologies were obtained by SEM in secondary electron mode. The wear track profiles were examined three times by a contact profilometer integrated to the tribometer and the coatings wear rates were calculated through the mean coating volume losses (mm³) divided by the normal force (N) and the total sliding distance (m) applied on the test.

3. Results and discussion

3.1 Morphology, chemical composition, and structure

Typical morphology and cross-section images of the Ti-(Si)-C-N nanocomposite coatings are shown in Figure 1. In general, the coated samples presented a cauliflower-like morphology with some nodular defects dispersed on the coating surface, as shown in detail in Figure 2. These common defects produced by PVD processes are concerned to lower the adhesion strength, fatigue and wear resistance of the as-deposited coatings by some authors [34,46,50]. Along with the TMS gas precursor addition, the surface morphology structures from Ti-C-N to Ti-Si-C-N system became less defined and slighted smaller while the cross-

sectional images revealed a change from columnar growth orientation to a dense and homogeneous form. Table 1 brings the EDS chemical composition of the as-obtained nanocomposite coated samples. The Ti-(Si)-C-N elemental compositions demonstrate close linear trends with the TMS flow rate. As expected, the content of Silicon and Carbon in the coatings is directly proportional to the amount of precursor flow rate with a decrease in the Titanium and residual Oxygen content. The Nitrogen amount remained constant for all coating conditions. The TiSiCN (3 g/h HMDSN) sample presented similar Silicon content of the TiSiCN (3.0 sccm TMS) sample but with much higher Carbon and lower Titanium amounts in the composition due to the high carbon content present in its precursor composition. Table 1 also presents the average values of surface roughness (Ra) for the coated samples. The roughness measurements verified a trend towards small Ra values for the coatings with higher Silicon and Carbon content. This roughness reduction agreed with the apparent coatings densification verified on the morphology images and the indicated refinement roles of Silicon and Carbon elements on the structure of TiSiCN nanocomposites.
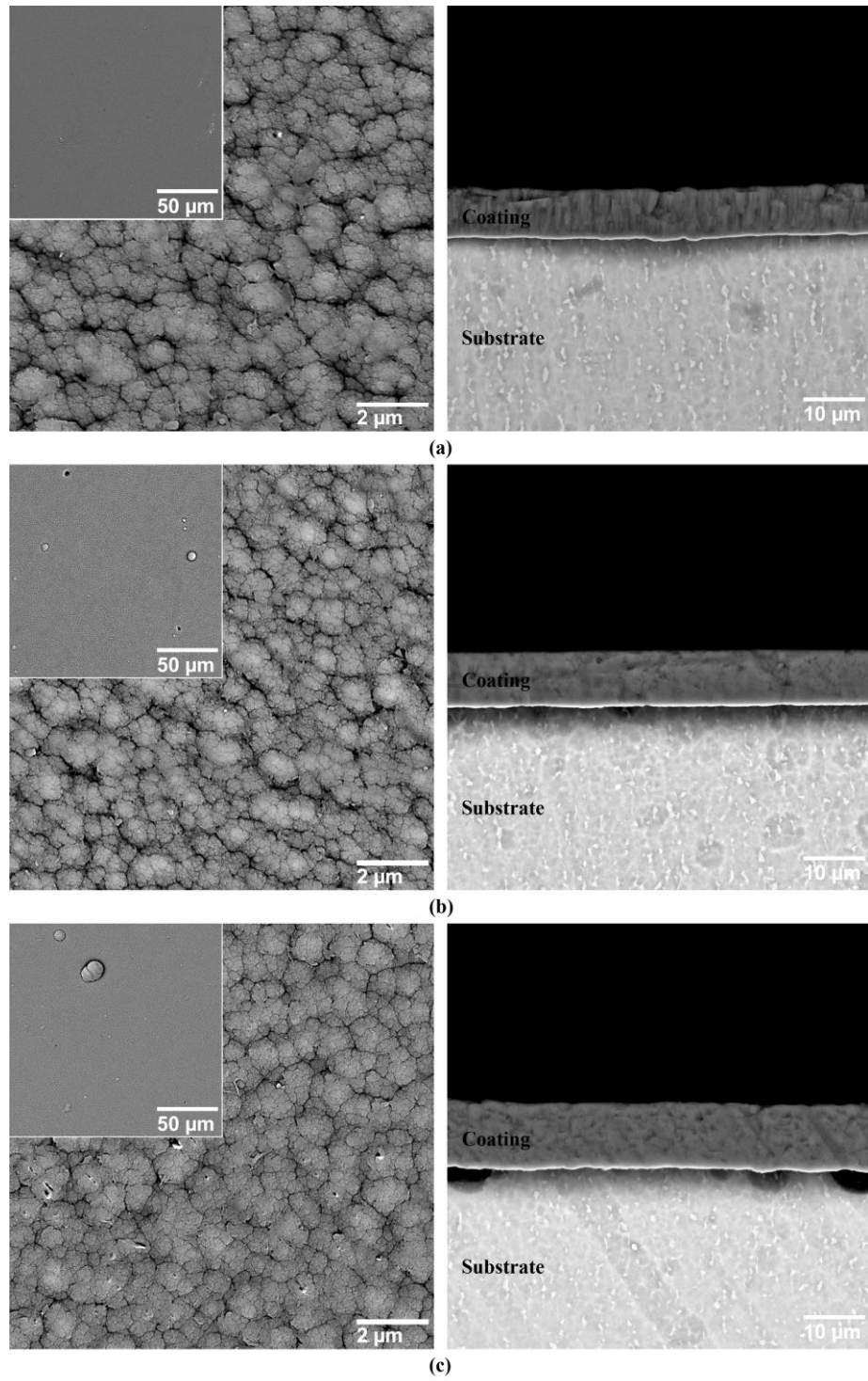
Figure 1 – Surface and cross-sectional SEM images of the samples (a) TiCN (0 sccm TMS), (b) TiSiCN (3.0 sccm TMS) and (c) TiSiCN (9.0 sccm TMS).
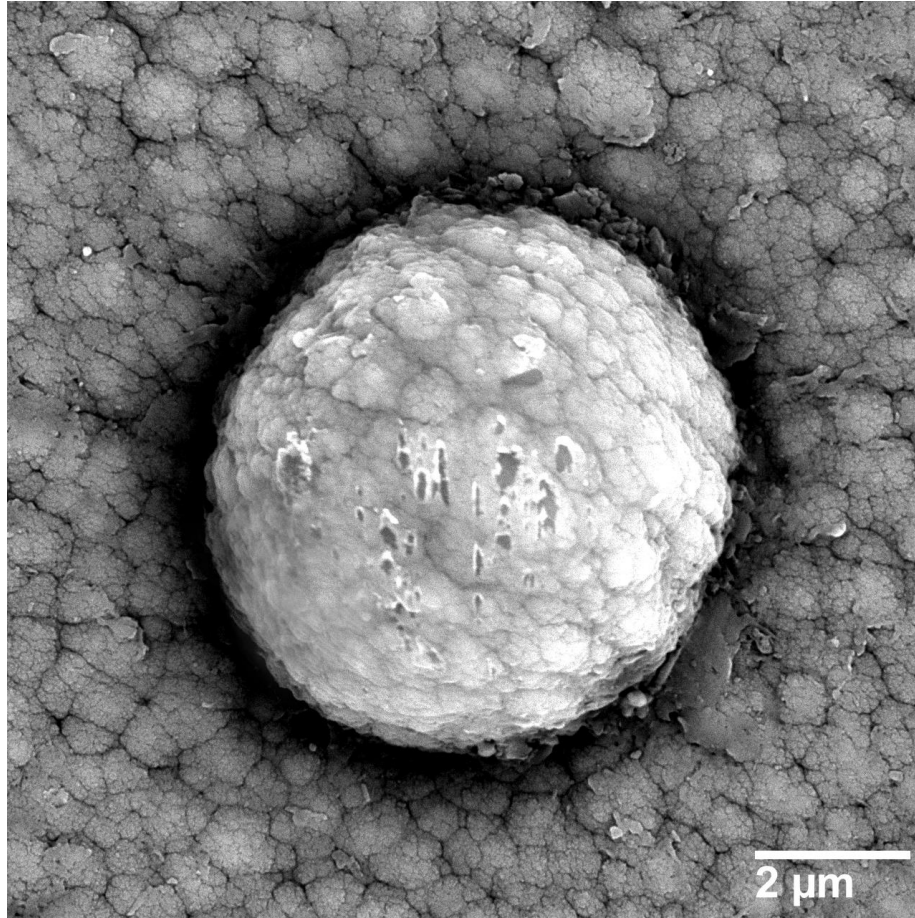
Figure 2 – High magnified SEM image of the typical nodular defect found dispersed on the coatings surface of all samples.

Table 3 – Chemical composition of the Ti-(Si)-C-N coatings as determined by EDS with estimated crystal size and mechanical parameters.

Sample	Chemical composition (at. %)					Roughness	Crystal size	H/E	H^3/E^2
	Ti	Si	C	N	O	(µm)	(nm)	(-)	(GPa)
TiCN (0 sccm TMS)	53.9	0	20.1	17.2	8.7	0.023	3.6	0.080	0.055
TiSiCN (1.5 sccm TMS)	48.8	1.4	24	16.3	9.5	0.020	3.5	0.084	0.059
TiSiCN (3.0 sccm TMS)	49.5	2.4	24.7	16.2	7.2	0.018	3.2	0.092	0.096
TiSiCN (6.0 sccm TMS)	47.3	4.3	26.2	17.8	4.4	0.017	3.0	0.096	0.112
TiSiCN (9.0 sccm TMS)	40.5	6.9	32.9	15.7	4.0	0.013	2.7	0.101	0.126
TiSiCN (3g/hr HMDSN)	37.6	2.6	37.7	13.4	8.6	0.018	2.9	0.091	0.088

XRD diffractograms are shown in Figure 3. All sample conditions have demonstrated five broad diffraction peaks addressed to the face-centered cubic (111), (200), (220), (311) and (222) crystallographic orientation from TiC_xN_y crystalline phase with

different stoichiometries. For instance, the peaks (111), (200), (220), (311) and (222) were indexed according to the $TiC_{0.3}N_{0.7}$ (ICDD PDF 00-042-1488) at 36.46°, 42.35°, 61.44°, 73.61° and 77.46°; the TiC (ICDD PDF 00-032-1383) at 35.91°, 41.71°, 60.45°, 72.37° and 76.14°; and the TiN (ICDD PDF 00-038-1420) at 36.66°, 42.60°, 61.81°, 74.07° and 77.96° diffraction patterns respectively. No Silicon compounds peaks could be verified on the XRD results. A preferred (200) orientation were evinced for all coated samples with a small broadening towards high values of Silicon and Carbon content. As these elements are increased, the peaks concisely enlarge, indicating smaller nanocrystallites on the coating structures. Similarly, the (200) orientation has been reported to be preferential in TiSiN coating systems obtained at high bias voltage due to its lowest surface energy position in B1 FCC structure and the high ion energy and mobility [51]. Therefore, the coatings have presented the (200) preferential orientation because of a high current density at the sample deposition surface, which has been reported to be 25 times greater in PEMS technique compared to CMS depositions [31]. In addition, the coatings crystallite sizes estimated by Scherrer formula are presented in Table 1. The nanocrystals size were found in a range from 3.6 to 2.7 nm. The influence of Silicon and Carbon as crystal refiners were verified on the Ti-Si-C-N structure. The Carbon role was evinced especially by comparing the 3.2 nm nanocrystal size of the TiSiCN (3.0 sccm TMS) sample to the 2.9 nm nanocrystal size of the TiSiCN (3g/h HMDSN), as both have similar Silicon content.
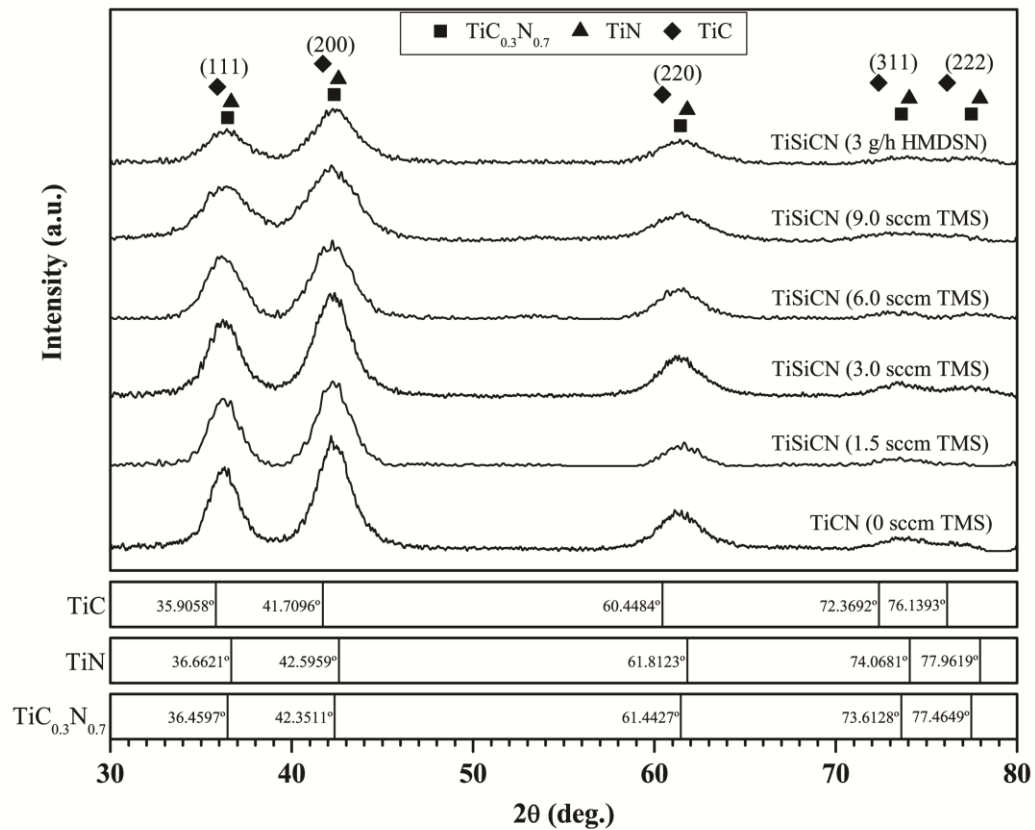
Figure 3 – XRD spectra of the nanocomposite Ti-(Si)-C-N coated samples.

Furthermore, the chemical state of the coatings was examined by XPS. The spectra for Ti 2p, Si 2p, C 1s and N 1s of the key condition coatings as the no silicon (TiCN, 0 sccm TMS), high silicon (TiSiCN, 9 sccm TMS) and high carbon (TiSiCN, 3 g/h HMDSN) contents are presented in Figure 4. The Ti 2p spectra were deconvoluted in five peaks, located around 454.5, 455.5, 457.6, 460.5 and 463.0 eV. The four fitting peaks located below 460.5 eV were addressed to be Ti(C, N) compounds [52–54]. Similar to the XRD results, the compounds identification can be difficult through XPS also, once the binding energies of the TiC and TiN compounds are very similar and the carbon and nitrogen atoms may substitute each other on the crystal structure, forming overlapped peak spectra due to the contribution of TiC_xN_y phases with different stoichiometries. The highest binding energy peak, at 463.0 eV can be associated with titanium oxides [55]. In the Si 2p spectra two fitting peaks centered at 101.5 and 102.4 eV were respectively indexed to Si_3N_4 [56] and SiO [57] phases. The influence of a high content of silicon can be verified by the strong signal of Si_3N_4 phase observed on the spectrum of the TiSiCN (9.0 sccm TMS) coating compared to the TiSiCN (3

g/h HMDSN) coating, this condition also resulted in a smaller estimation size of the TiCN nanocrystals in the XRD analyses. Thus, a high silicon content is supposed to refine the nanocrystals by enlarging the Si_3N_4 amorphous matrix on TiSiCN system. The C 1s spectra were composed by the contributions of Ti-C at 281.7 eV [58,59], C-C sp2 at 284.2, C-C sp3 285.2 eV and C=O at 288.0 binding energies [60–62]. The outstanding C-C fitting peaks revealed on the coatings spectra present similar responses from the carbon hybridization states found on DLC coatings, and thus suggest the formation of these structures within the nanocomposite. For instance, the sp2 and sp3 bonding are respectively associated to the graphitic and diamond fractions present in DLC coatings, which are responsible to provide improved mechanical properties with a low coefficient of friction [63,64]. The amount of each bonding fractions present in the coatings can be estimated through the area ratio between the indexed sp2 and sp3 fitting curves [62]. The estimation conferred an amount of 53, 65 and 68 % of sp2 bonding sites for the TiCN (0 sccm TMS), TiSiCN (9 sccm TMS) and TiSiCN (3 g/h HMDSN) coated samples respectively. These results demonstrated a linear correlation between the carbon content presented in the coatings chemical composition and the fraction of sp2 bonding. At this point, the TiSiCN (3 g/h HMDSN) sample is expected to present the smaller coefficient of friction during the rubbing test comparing to the other samples, mainly due to its higher amount of graphitic bonding fraction present, which is intended to act as a solid lubricant on the surfaces in contact. Finally, the N 1s spectra demonstrate responses of C-N bondings at 399.9 eV [65], Si_3N_4 at 397.9 eV [66] and the TiCN in the region from 395.2 to 396.5 eV [67], which this region can be explained again by the carbon substitution of nitrogen and vice-versa on the crystal lattice.
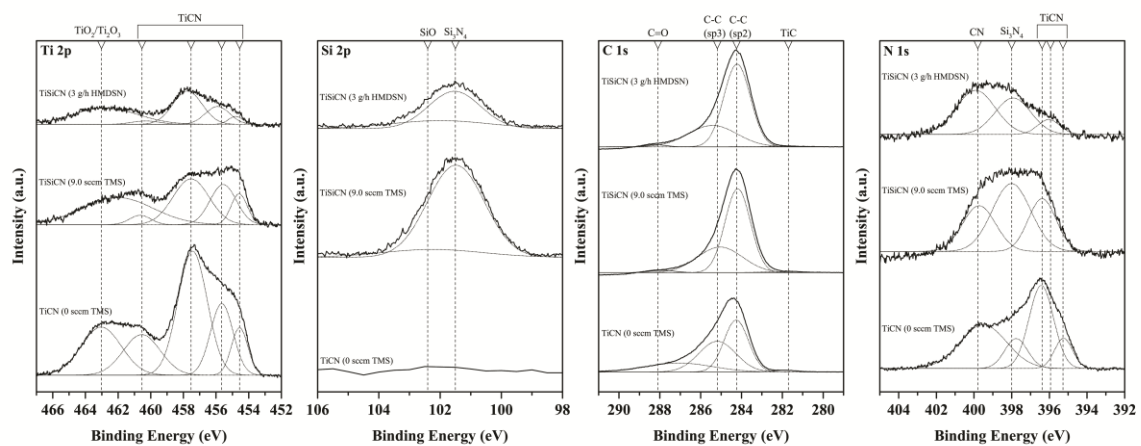

Figure 4 – XPS spectra at Ti 2p, Si 2p, C1s and N 1s bias voltage of the TiCN (0 sccm TMS), TiSiCN (9.0 sccm TMS) and TiSiCN (3 g/h HMDSN) coated samples.

These results were found in good agreement with recently selected area diffraction patterns (SAED) studies and high-resolution transmission electron microscopy (HRTEM) performed in TiSiCN coatings [42,68]. In these studies, authors verified the phase segregation of a polycrystalline Ti(C,N) structure embedded in a thin amorphous matrix of Si_3N_4 and sp2 amorphous carbon in the TiSiCN coating structure. Similarly to the densification verified in cross-sectional images in Figure 1, the evolution from columnar to dense nanocomposite structure within an increasing of Silicon and Carbon content were confirmed in the TiSiCN coatings.

3.2 Mechanical properties and adhesion strength

Figure 5 present the hardness and the elastic modulus as a function of indentation depth by means of nanoindentation for the low friction Ti-(Si)-C-N nanocomposite coatings. The samples hardness were found in a range of 7 to 14 GPa, with a strong correlation to the nanocrystallites size estimated on the coating structures. The hardness values are found in good agreement with other low friction Ti-Si-C-N coating systems deposited with C_2H_2 [32]. Also, similar enhancement of hardness within structure refinement was observed in Ti-Si-C-N coating systems with silicon content below 8 at. % [40]. This hardening effect towards smaller nanocrystal size can be mainly explained by an enhanced cohesive strength of the nanocrystallites boundaries in the refined structure, which impose a structure restriction to the movements and dislocations of the phases in response to deformation. In addition, other factors may contribute to the coatings hardness enhancement as residual stress, coating densification and morphology [42,44]. Despite the similar nanocrystallites size value, the Ti-Si-C-N (3 g/h HMDSN) sample presented lower hardness mean values compared to the Ti-Si-C-N (3.0 sccm TMS). This is attributed to a fragilization effect introduced by a greater content of the soft amorphous carbon region within the coating structure on such coating [32,35]. Similarly, the elastic modulus values have followed the hardness order of the coated samples. Accordingly, the hardness and the modulus of elasticity demonstrated to be very dependent on the nanocrystallites sizes in the Ti-Si-C-N nanocomposites coated samples. This statement is found in good agreement with the idealized model of ultrahard nanostructured film proposed by some authors [36,69,70].
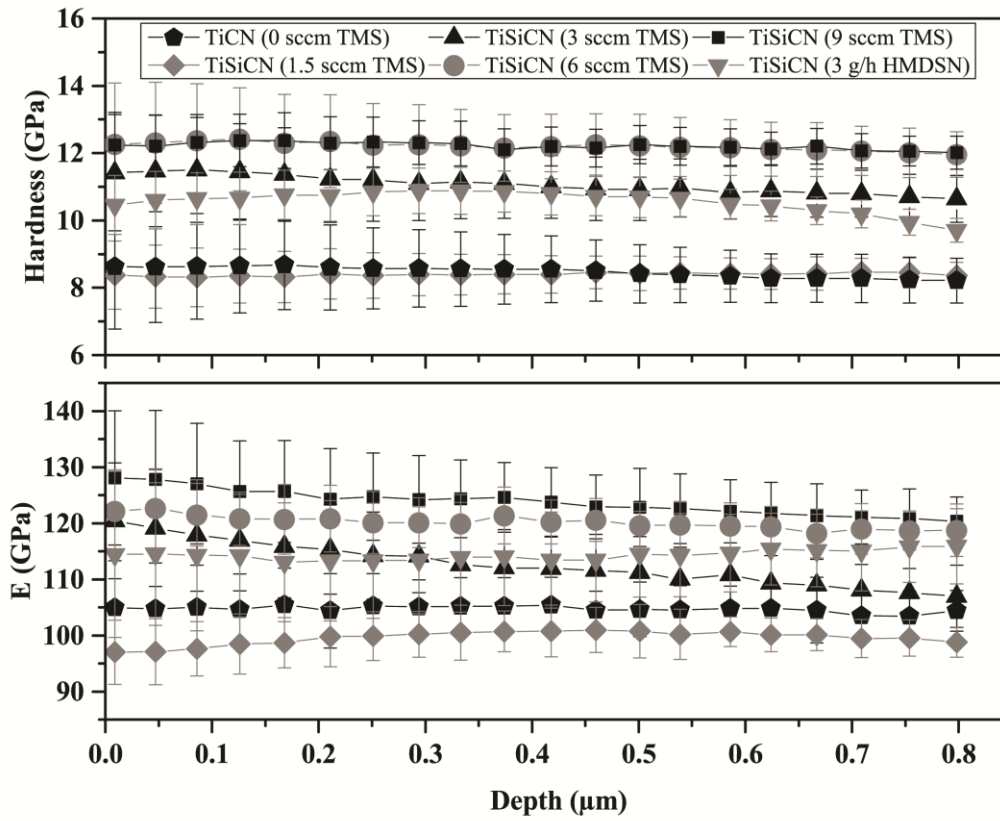
Figure 5 – Hardness and elastic modulus profile for the Ti-(Si)-C-N coated samples.

In addition, Table 1 brings the resistance to elastic strain to failure (H/E) and the resistance to plastic deformation (H^3/E^2) parameters of the Ti-(Si)-C-N samples. These parameters have been used as important mechanical performance indicators in nanostructured coatings due to a fine correlation with the resistance to cracking and wear [71,72]. The results demonstrated that the parameters are linked to the silicon and carbon content in all the Ti-(Si)-C-N coated samples and hence to the structure refinement verified by the nanocrystallites sizes. Consequently, the highest values of H/E and H^3/E^2 were found in the Ti-Si-C-N (9 sccm TMS) sample, 0.101 and 0.126 respectively. The significance of the resistance to elastic strain to failure and the resistance to plastic deformation are evident in the critical loads obtained by the scratch adhesion test of the coated samples, which are shown in Figure 6 and subsequently discussed. As these critical loads (L_C) are determined at the normal load applied in the first occurrence points of cohesive (L_{C1}) and adhesive (L_{C2}) failures during the test, they present to be intrinsically related to the mechanical parameters H/E and H^3/E^2.

Thereby, the adhesion strength of the Ti-(Si)-C-N nanocomposite coatings were quantitatively assessed by scratch adhesion test following the ASTM C1624-05 Standard [49]. This test typically consists of a defined geometry indenter pulling across the coated sample surface at a constant speed with an applied progressive normal force, which then provokes mechanical damages in the coating and the substrate. For instance, in this study was determined two-level critical loads (L_C) defined as the applied normal load at the first occurrence points of the cohesive (L_{C1}) and the adhesive (L_{C2}) failures of the Ti-(Si)-C-N coated samples. These failures were identified by optical microscopy and then classified according to the scratch atlas annex presented the ASTM C1624-05 Standard [49]. The assigned critical loads and failure modes presented in the coated samples are compared in Figure 6. The Ti-Si-C-N (9 sccm TMS) have demonstrated the highest critical loads values for both failures modes among all the samples. This result was expected as this coating presents the superior values for the resistance to elastic strain to failure and plastic deformation. In this case, high H/E and H^3/E^2 ratios have been considered effectively to prevent crack formation and propagation on nanostructure coatings [73]. Moreover, a considerable cohesive strength enhancement has been verified in the nanocomposite structure of Ti-Si-C-N compared to Ti-C-N, which is revealed by the large increment in the L_{C1} value from the TiCN (0 sccm TMS) to the TiSiCN (1.5 sccm TMS) samples. Naturally, the columnar structure verified on TiCN (0 sccm TMS) introduce, as-deposited, defects that act as crack nucleation sites when the coating is stressed. In fact, the critical loads measurement is susceptible to many intrinsic (i.e. scratch test parameters and equipment) and extrinsic (i.e. coating and substrate properties) factors of scratch testing [74]. Therefore, an optimal refined structure, as demonstrated in Ti-Si-C-N (9.0 sccm TMS) coated sample, was verified as a fundamental requirement to provide a well adhered Ti-Si-C-N nanocomposite coating.
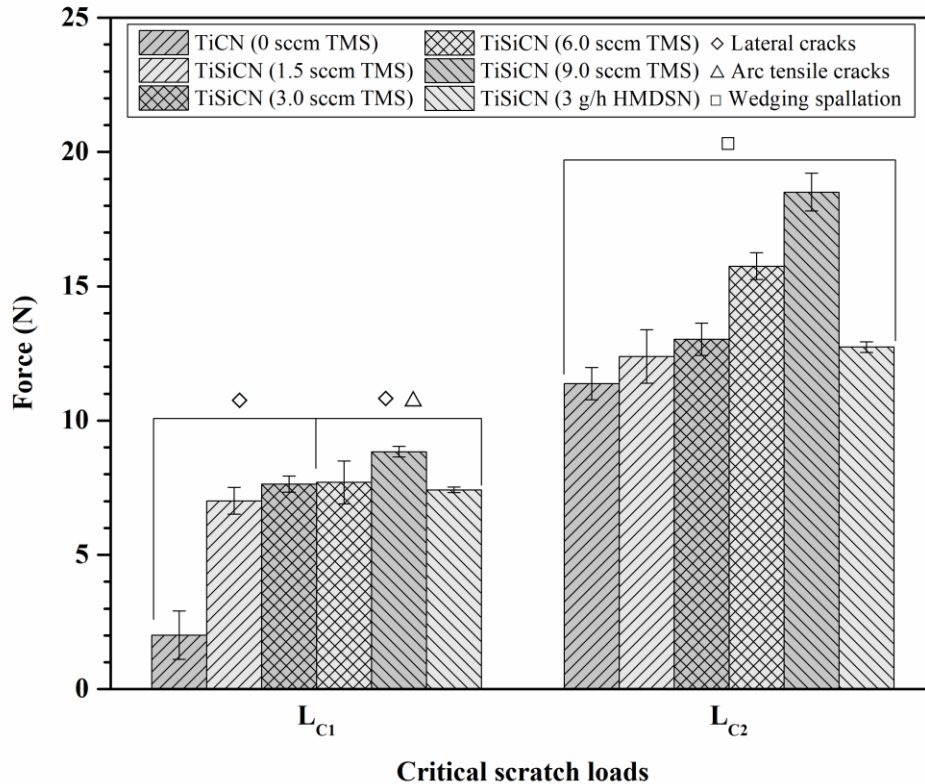
Figure 6 - Critical loads and failures modes from scratch test on the Ti-(Si)-C-N coated samples.

Despite the quantitative results, it is also possible, during the scratch test, to monitor the tangential force, friction coefficient, acoustic emission, profile and residual depths as a function of the applied normal load and test distance. These responses not only assist the critical load points determination but also may provide relevant information of damages mechanisms and coating system elastic recovery. Therefore, Figure 7 presents a complete response graph indexed to the scratch optical image of the Ti-Si-C-N (9.0 sccm TMS) sample. As shown, the scratch test could be divided into four distinct regions. In the first region, which is defined prior to the first cohesive failure occurrence (left from the L_{C1} line), an increase of a quivered friction coefficient with low acoustic emission signals are observed within the increase on the applied normal force. This is a common response attributed to asperities remotion from the coating surface by the indenter. Then, a second region could be defined from the first occurrence of the cohesive failure until the adhesive failure (between the L_{C1} and L_{C2} lines). In the second region, the friction coefficient continues to increase in

the same slope from the test starting and tiny variations on the acoustic emission signal were perceived as cracking occurs in the coating. However, an accuracy value of first critical load had claimed high magnification optical microscope images for all coated samples analysis. The wedging spallation adhesive failure can well define the third region until the substrate exposure (between L_{C2} line and substrate exposure line). The L_{C2} line is well defined by a steep rise, on both, friction coefficient and acoustic emission signals with high amplitude peaks until substrate exposure. These are responses related to the regularly spaced wedging spallation besides the scratch trail, which occurs when the lateral cracks assume a critical length that provokes a delamination of the TiSiCN film exposing the TiN interlayer. Moreover, plastic deformation occurs from this point until the end of the test as demonstrated by the residual depth measurement. Finally, the last region defined by substrate exposure which exhibits an increase in residual depth and very high coefficient of friction due to a bigger penetration area in front of the indenter. The other Ti-(Si)-C-N coated samples presented similar response behavior, with four regions well defined but critical loads lines assigned at lower values of applied normal force.
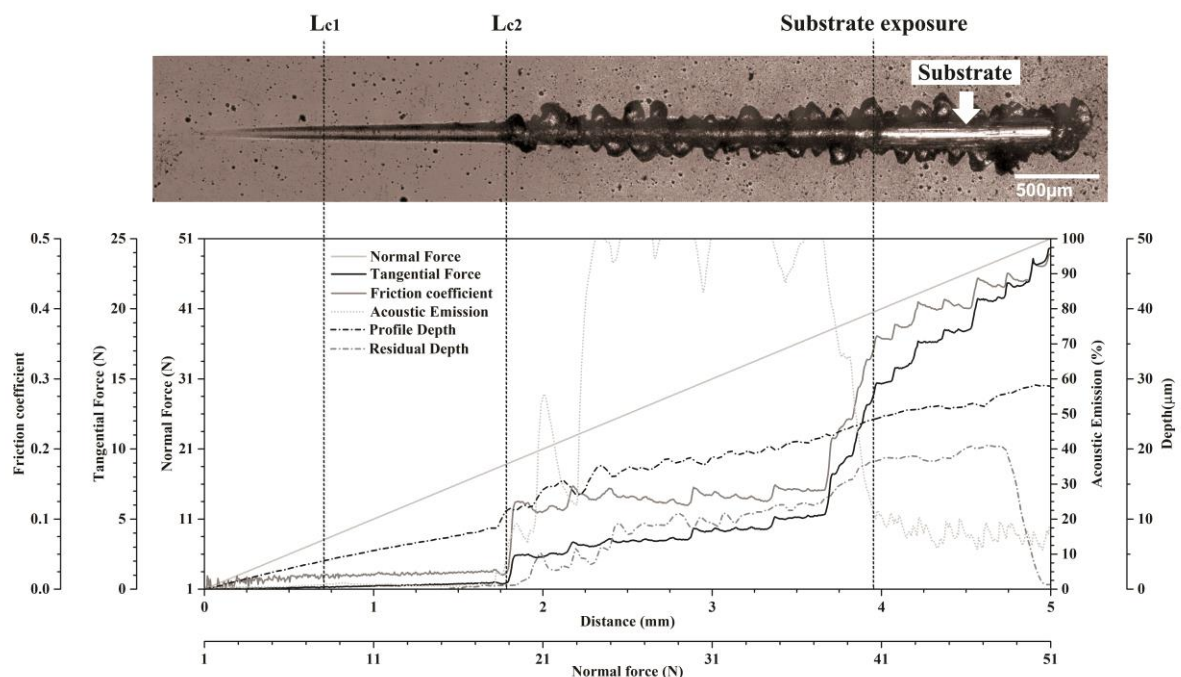

Figure 7 – Scratch test optical image indexed to the graph of monitored responses as a function of the applied normal force and scratch distance of the Ti-Si-C-N (9.0 sccm TMS) coated sample.

Furthermore, Figure 8 brings high magnification images of the cohesive and adhesive failures identified in the Ti-Si-C-N (9.0 sccm TMS) coated. As described, this coating sample has presented lateral cracks within arc tensile cracks inside the scratch trail as a cohesive failure mode. Both are typically brittle failures modes in a scratch test that may arise from the response to the tensile stresses introduced by the rear of the indenter [75]. Therefore, when these cracks overlap in a critical length, a spallation may occur in the interface between the Ti(Si)CN film and the bonding interlayer. The "shell" form of this spallation, observed at the right image in Figure 8, assign this adhesive failure as wedging spallation damage. Again, this is a failure response from brittle coating and substrate system and is generated by the internal stresses energy releasing due elastic recovery of the Ti(Si)CN film behind the moving indenter during the scratch test [75]. The arc tensile cracks were not observed in the Ti(Si)CN (0, 1.5 and 3.0 sccm TMS) coated samples, highlighting the role of higher Silicon and Carbon content on coating embrittlement. In summary, the coating cracking with interface failure observed in scratch test results categorize all the coated samples with good interface bonding according to the ASTM C1624–05 Standard [23]. Therefore, the adhesion results demonstrated that low friction Ti(Si)CN coated samples have attended a fundamental requirement to succeed in load-bearing biomedical applications.
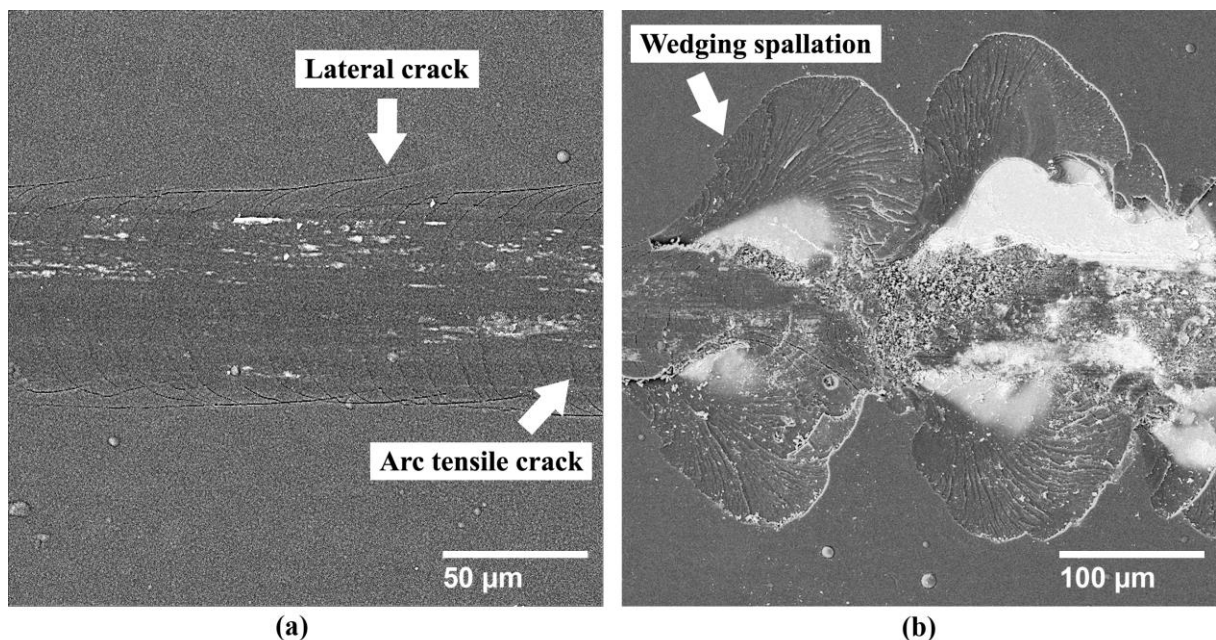

Figure 8 – Partially magnified optical images of the scratch test failures, cohesive at left and adhesive at right, with the identified damage terms of the Ti-Si-C-N (9.0 sccm TMS) coated sample.

3.3 Tribocorrosion test

Figure 9 shows the monitored OCP measurement before, during and after the tribocorrosion reciprocal sliding tests, in PBS solution, for the samples of Ti-(Si)-C-N coatings and Ti-6Al-4V bare alloy. All coated samples improved the corrosion resistance in comparison with the uncoated titanium alloy with stable corrosion potential in anodic level, as demonstrated in the steady region before the rubbing period. Moreover, nobler properties were verified on the Ti-Si-C-N coated samples within higher silicon and carbon content. Similar enhancement in corrosion resistance related to smaller crystallites size in an amorphous matrix has been reported in of TiSiC-Cr and TiSiC-Zr coatings [76]. This effect is mainly attributed to the coatings densification, which the amorphous matrix acts as a barrier to the nanocrystallites boundaries against the corrosive environment. At the beginning of rubbing, the Ti-6Al-4V uncoated sample presented a typically large drop on OCP towards cathodic direction due to the removal of the passive titanium oxide layer in the sliding track area. As the test runs, noise OCP signal is acquired, which are a response from the successive passivation and the passive film removal in the titanium alloy exposed regions during the reciprocal sliding movement [77]. The Ti-(Si)-C-N (0, 1.5 and 3.0 sccm TMS) samples have shown a similar behavior of the Ti-6Al-4V uncoated sample within minor scale drop values, indicating the removal of corrosion protective film layer. Moreover, some pronounced valleys could be observed, for instance in the Ti-Si-C-N (1.5 sccm TMS) coating, which might be attributed to significant damages provoked on the coatings and verified later on in the SEM images of the wear tracks. In case of the Ti-Si-C-N (3.0 sccm TMS) sample, some small valleys were identified in the OCP signal until the 300 seconds of the tribocorrosion test, at this the OCP drops significantly indicating a synergistic effect of corrosion and wear in the coating failure. On the other hand, the rest of samples remained absent of potential drops during the tribocorrosion reciprocal sliding test, which was verified later as an indicator of coating integrity. As the movement ceases, the passivation effect is shown by the curve towards to the value of OCP stabilizing period in the affected samples while in the other samples almost no variation was registered in the OCP. Additionally, previous tribocorrosion reciprocal sliding test with loads lower than 10 N exhibited no variation in the OCP of all the coated samples.
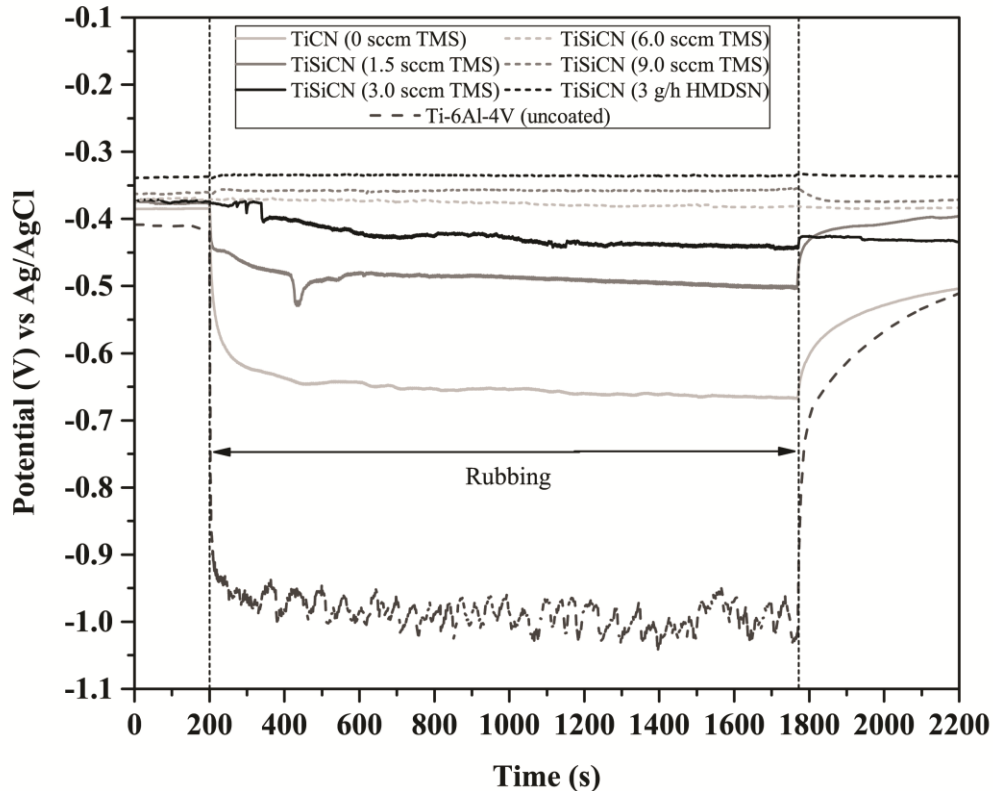
Figure 9 - Monitored OCP measurements before, during and after tribocorrosion reciprocal sliding test in 1× PBS solution for the Ti-(Si)-C-N coated and Ti-6Al-4V uncoated samples.

Moreover, the Ti-Si-C-N (9.0 sccm TMS) demonstrated an abnormal anodic behavior in the OCP compared to the other samples during the rubbing period. The slight shift in OCP towards anodic direction observed suggests a higher silicon oxide generation and releasing into the adjacent electrolyte due to the extensive silicon nitride (Si_3N_4) matrix presented in the Ti-Si-C-N (9.0 sccm TMS) compared to the others samples. In fact, Bal and Rahaman [78] investigated the complex wear mechanism of silicon nitride (Si_3N_4) ceramics for orthopedic applications and verified a synergic contribution of mechanical and tribochemical wear modes on this material. In this case, primary oxides and silicon nitride debris are removed from the surface by mechanical abrasion which then reacts with the electrolyte generating silicon oxides (SiO_2) and also hydrated silicon oxide ($Si(OH)_4$). This last may form a comprised lubricating film between the sliding surfaces that are in continuous movement regimes with higher speeds and lower loads, which contributes to a lower coefficient of friction and wear rate verified afterward. At the rubbing ending, the debris

releasing stops and the silicon reduction reactions occurs, turning slowly the OCP value to the stabilization level as observed by a small convex curve observed in Figure 9. Although this might be occurring in all samples within titanium ions releasing, the oxidation reactions seem to be augmented by the Ti-Si-C-N (9.0 sccm TMS) sample structure and overlapping the cathodic responses as observed in the other samples.

The wear tracks surface SEM images for all the samples are presented in Figure 10. The images revealed a well-defined trend towards small wear track widths from TiCN (0 sccm TMS) to TiSiCN (9.0 sccm TMS) samples. Surface failures, such as cracking and delamination, are visible on the coated samples Ti(Si)CN (0, 1.5 and 3.0 sccm TMS). These failures are well correlated with the OCP responses for those coatings. Moreover, micrometer-sized detachments could be observed inside the track trails of the TiSiCN (6.0 and 9.0 sccm TMS) samples, which is intrinsic to the fatigue wear mechanism. No failure was noticed in the TiSiCN (3 g/h HMDSN), however, a high amount of debris beside a much-smoothed track surface were verified when compared to the other samples. In fact, the verified mechanical properties, adhesion strength, and coting structure have demonstrated to play an important role in the tribocorrosion performance of such nanocomposite coatings. For instances, the TiSiCN (9.0 sccm TMS) have presented the smallest track width within the samples, indicating a minimum inward movement of the counter-body ball into the coating sliding surface. Conversely, the TiCN (0 sccm TMS) coated sample exhibited an extensive damage along all the wear track surface. For this reason, the tribocorrosion behavior is greatly improved by the silicon amorphous matrix present on the nanocomposite structure, which restrains the combined action of wear and corrosion mechanisms by an eradication of the intrinsic defects from a columnar coating structure. Furthermore, the high fraction of sp2 clusters in the TiSiCN (3 g/h HMDSN) sample provides an enhanced self-lubrication effect of its surface. As this graphite-like structure present poor shear resistance, it is easily removed from the sliding surfaces, resulting in the generation of the high amount of surrounded debris. Nevertheless, all coating conditions indicate improved tribocorrosion resistance due to a clear reduction in track widths and the absence of the abrasive grooves as demonstrated in the wear track of the titanium bare alloy sample.
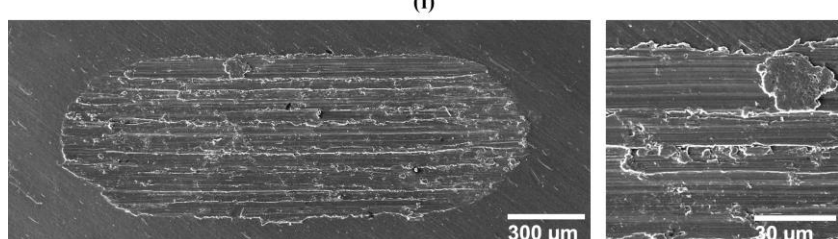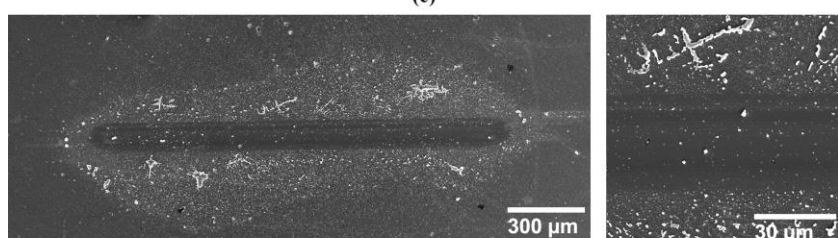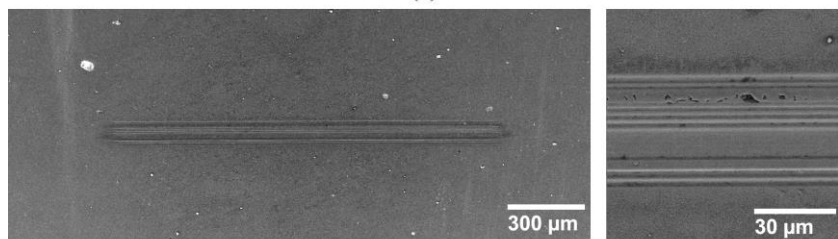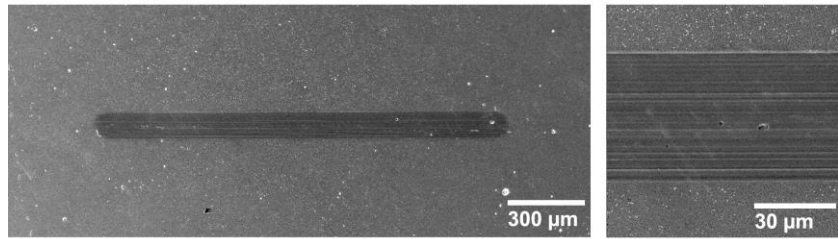
(a)

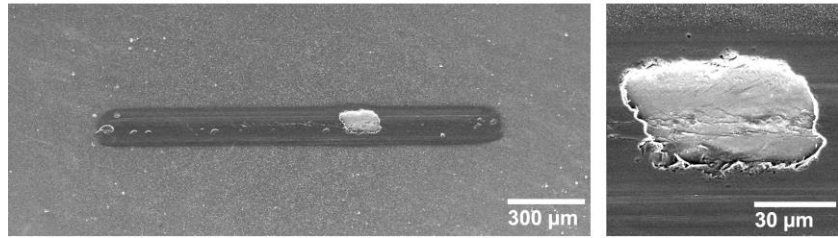(b)

(c)

(d)

(e)

(f)

(g)
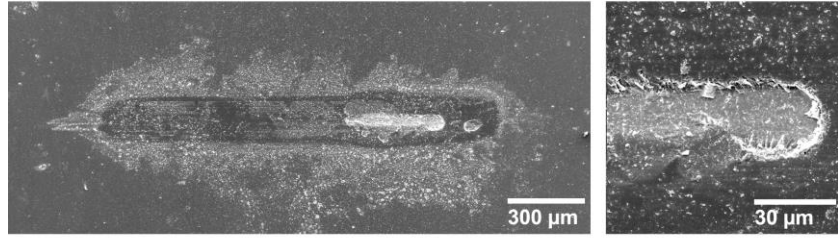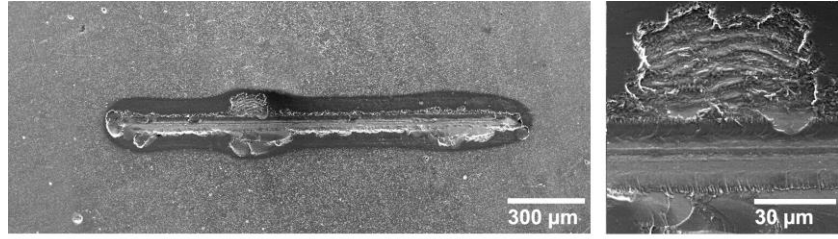
Figure 10 – SEM images of the tribocorrosion wear tracks at left and center track enlarged at right for the samples (a) TiCN (0 sccm TMS), (b) TiSiCN (1.5 sccm TMS), (c) TiSiCN (3.0 sccm TMS), (d) TiSiCN (6.0 sccm TMS), (e) TiSiCN (9.0 sccm TMS), (f) TiSiCN (3 g/h HMDSN) and (g) Ti-6Al-4V uncoated.

Figure 11 shows the coefficient of friction (COF) monitored during the sliding in the tribocorrosion tests in the Ti-(Si)-C-N nanocomposite coatings and the uncoated titanium samples. The low friction nanocomposite coated samples presented COF between 0.17 and 0.20 against the Al2O3 ball immersed in PBS on the steady-state regime. These values are much lower when compared to the ~0.40 obtained in the titanium alloy sample at the end of the test. In addition, shorter running-in distances were conferred in the coated samples compared to the uncoated titanium alloy sample. Besides the better surface finishing of coatings, this behavior can be attributed to the lubrication of the proposed carbon transfer layers formed between the sliding surfaces. This carbon transfer layer has been proved to lower the friction coefficient of the TiSiCN coatings, even under corrosive environment, through the deposition onto the tribo-pair and acting as a solid lubricant on the sliding surfaces [42]. Therefore, the coated samples with higher carbon content, TiSiCN (6.0, 9.0 sccm TMS and 3 g/h HMDSN), presented slightly lower COF values at the end of a test than the others samples. Also, much less noise in the COF signals are perceived on those coatings due to much less contribution of abrasive wear mechanism. Forasmuch, as verified in the XPS analysis, the large amount of graphitic fraction resulted in the smaller COF of the TiSiCN (3 g/h HMDSN) between all the samples. Furthermore, the damaged coated samples observed in SEM images have presented broaden elevation within the first meters of the reciprocal sliding test. These were associated with the damages verified in Figure 10. As the damage occurs, an abrupt increase in the COF is perceived, thus new boundaries asperities are formed from the delaminated area requiring certain sliding cycles to accommodate the counter-ball again.
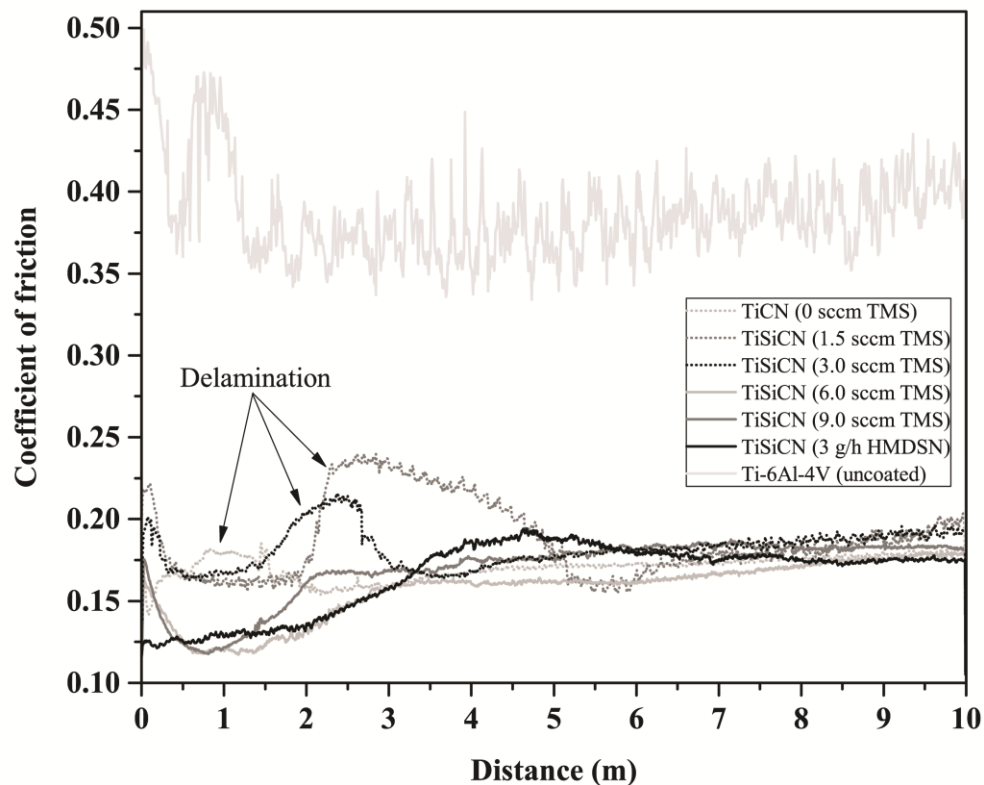
Figure 11 - Coefficient of friction during the tribocorrosion reciprocal sliding test against Al_2O_3 sphere in $1\times$ PBS solution for the Ti-(Si)-C-N coated and Ti-6Al-4V uncoated samples.

Finally, Figure 12 presents the obtained tribocorrosion wear rates of all tested samples. The wear rate values revealed a strong decrease within the Ti-(Si)-C-N nanocomposite coating application compared to the uncoated titanium sample. The wear rate remained in values from 6.81×10^{-6} to 7.56×10^{-7} mm³/N/m for the coated samples and 2.61×10^{-4} for the uncoated titanium sample. The smallest wear rate value was found in the Ti-Si-C-N (9.0 sccm TMS) followed by the Ti-Si-C-N (3g/h HMDSN) samples. Also, the graph shows the strong effect of the delamination which triples the wear rate in comparison with the undamaged coatings. The wear rate values obtained on the nanocomposite coated samples were found to be much smaller than those found on DLC-coated Ti-6Al-4V alloy under similar tribocorrosion test [21]. In summary, the results have confirmed that a number of factors may imply on the tribocorrosion performance of the studied nanocomposite coatings. The improved mechanical properties, adhesion strength, electrochemical stability and low friction coefficient responses have indicated the TiSiCN (9.0 sccm TMS) sample shows the best

tribocorrosion behavior among all samples. The good tribocorrosion performance obtained by the high carbon content TiSiCN (3 g/h HMDSN) sample also highlighted the role importance of self-solid lubrication capability of the amorphous carbon regions within the coatings structure. At the end, the low friction TiSiCN nanocomposite coatings examined presented much lower wear rates and COF values compared to usual biomedical titanium alloy under PBS solution.
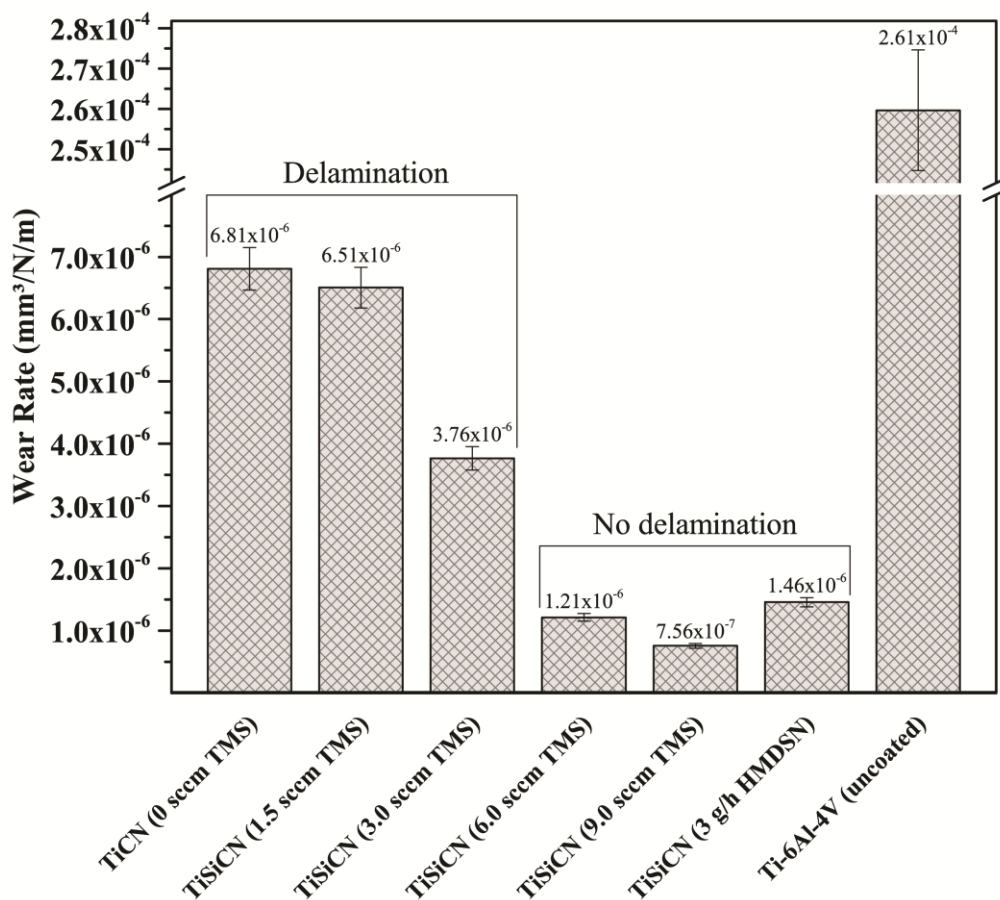
Figure 12 - Wear rate obtained from the loss volume of the tribocorrosion reciprocal sliding test in $1\times$ PBS solution for the Ti-(Si)-C-N coated and Ti-6Al-4V uncoated samples.

4. Conclusions

The tribocorrosion behavior of low friction Ti-(Si)-C-N nanocomposite coatings deposited on titanium alloy under PBS was studied. The low friction Ti-(Si)-C-N nanocomposite coatings have presented an expressive reduction of at least 97% in the wear rate of the usual biomedical ASTM F136 titanium alloy. Moreover, the tribocorrosion performance of the coated samples demonstrated strong correlation within many factors

governed by the as-obtained coating chemical composition and nanostructure, which was verified to be composed by Ti(C)N nanocrystallites embedded in a Si_3N_4 amorphous matrix within dispersed carbon amorphous sites. For instance, the nanocrystallites refinement was proven to enhance the coating mechanical properties and therefore the adhesion strength by increasing the elastic strain to failure (H/E) and plastic deformation (H^3/E^2) indexes. Among the applied PEMS depositions, the optimal coating condition obtained with flow rates of 9.0 sccm TMS and 30 sccm C_2H_2 was verified. These conditions conferred the best response to the synergistic activity of corrosion and wear during the tribocorrosion tests. In addition, the role of carbon in the self-solid lubrication capability of the coating amorphous carbon sites was highlighted. In conclusion, the low friction Ti-Si-C-N nanocomposite coating, within an optimal condition, was confirmed as a strongly adhered coating to enhance the tribocorrosion behavior in the physiological environment and thus attend the demanded extension in the lifespan of titanium alloy biomedical applications.

Acknowledgments

References

[1]   M.A. McGee, D.W. Howie, K. Costi, D.R. Haynes, C.I. Wildenauer, M.J. Pearcy, J.D. McLean, Implant retrieval studies of the wear and loosening of prosthetic joints: A review, Wear. 241 (2000) 158–165. doi:10.1016/S0043-1648(00)00370-7.

[2]   M.T. Mathew, P. Srinivasa Pai, R. Pourzal, A. Fischer, M.A. Wimmer, Significance of tribocorrosion in biomedical applications: Overview and current status, Adv. Tribol. 2009 (2009). doi:10.1155/2009/250986.

[3]   J. Villanueva, L. Trino, J. Thomas, D. Bijukumar, D. Royhman, M.M. Stack, M.T. Mathew, Corrosion, Tribology, and Tribocorrosion Research in Biomedical Implants: Progressive Trend in the Published Literature, J. Bio- Tribo-Corrosion. 3 (2017) 1. doi:10.1007/s40735-016-0060-1.

[4]   J. Raphel, M. Holodniy, S.B. Goodman, S.C. Heilshorn, Multifunctional coatings to simultaneously promote osseointegration and prevent infection of orthopaedic implants., Biomaterials. 84 (2016) 301–314. doi:10.1016/j.biomaterials.2016.01.016.

[5]   N.J. Hallab, J.J. Jacobs, Biologic effects of implant debris, Bull. NYU Hosp. Jt. Dis. 67 (2009) 182–188.

[6]   A. Sargeant, T. Goswami, Hip implants: Paper V. Physiological effects, Mater. Des. 27 (2006) 287–307. doi:10.1016/j.matdes.2004.10.028.

[7]   S. Desai, B. Bidanda, P. Bártolo, Metallic and Ceramic Biomaterials: Current and Future Developments, in: P. Bártolo, B. Bidanda (Eds.), Bio-Materials Prototyp. Appl. Med., 1st ed., Springer US, 2008: pp. 1–14. doi:10.1007/978-0-387-47683-4.

[8]   V. Gopal, M. Chandran, M.S.R. Rao, S. Mischler, S. Cao, G. Manivasagam, Tribocorrosion and electrochemical behaviour of nanocrystalline diamond coated Ti based alloys for orthopaedic application, Tribol. Int. 106 (2017) 88–100. doi:10.1016/j.triboint.2016.10.040.

[9]   P. Sadoghi, M. Liebensteiner, M. Agreiter, A. Leithner, N. Böhler, G. Labek, Revision surgery after total joint arthroplasty: A complication-based analysis using worldwide arthroplasty registers, J. Arthroplasty. 28 (2013) 1329–1332. doi:10.1016/j.arth.2013.01.012.

[10]   P. Herberts, H. Malchau, Long-term registration has improved the quality of hip replacement: a review of the Swedish THR Register comparing 160,000 cases., Acta Orthop. Scand. 71 (2000) 111–121. doi:10.1080/000164700317413067.

[11]   O. Robertsson, K. Knutson, S. Lewold, L. Lidgren, The Swedish Knee Arthroplasty Register 1975-1997: an update with special emphasis on 41,223 knees operated on in 1988-1997., Acta Orthop. Scand. 72 (2001) 503–13. doi:10.1080/000164701753532853.

[12]   M. Browne, P.J. Gregson, Metal ion release from wear particles produced by Ti-6Al-4V and Co-Cr alloy surfaces articulating against bone, Mater. Lett. (1995). doi:10.1016/0167-577X(95)00082-8.

[13]   M. Geetha, A.K. Singh, R. Asokamani, A.K. Gogia, Ti based biomaterials, the ultimate choice for orthopaedic implants - A review, Prog. Mater. Sci. 54 (2009) 397–425. doi:10.1016/j.pmatsci.2008.06.004.

[14]   N.J. Hallab, S. Anderson, M. Caicedo, A. Brasher, K. Mikecz, J.J. Jacobs, Effects of soluble metals on human peri-implant cells, J. Biomed. Mater. Res. Part A. 74A (2005) 124–140. doi:10.1002/jbm.a.30345.

[15]   T.S.N. Sankara Narayanan, Nanocoatings to improve the tribocorrosion performance of materials, 2012. doi:10.1016/B978-1-84569-949-9.50008-3.

[16]   T.T. Liao, T.F. Zhang, S.S. Li, Q.Y. Deng, B.J. Wu, Y.Z. Zhang, Y.J. Zhou, Y.B. Guo, Y.X. Leng, N. Huang, Biological responses of diamond-like carbon (DLC) films with different structures in biomedical application, Mater. Sci. Eng. C. 69 (2016) 751–759. doi:10.1016/j.msec.2016.07.064.

[17]   G. Dearnaley, J.H. Arps, Biomedical applications of diamond-like carbon (DLC) coatings: A review, Surf. Coatings Technol. 200 (2005) 2518–2524. doi:10.1016/j.surfcoat.2005.07.077.

[18]   A. Revathi, S. Magesh, V.K.V.K. Balla, M. Das, G. Manivasagam, Current advances in enhancement of wear and corrosion resistance of titanium alloys – a review, Mater. Technol. 31 (2016) 1–9. doi:10.1080/10667857.2016.1212780.

[19]   Z.A. Uwais, M.A. Hussein, M.A. Samad, N. Al-Aqeeli, Surface Modification of

Metallic Biomaterials for Better Tribological Properties: A Review, Arab. J. Sci. Eng. 42 (2017) 4493–4512. doi:10.1007/s13369-017-2624-x.

[20] G. Gotzmann, J. Beckmann, C. Wetzel, B. Scholz, U. Herrmann, J. Neunzehn, Electron-beam modification of DLC coatings for biomedical applications, Surf. Coatings Technol. 311 (2017) 248–256. doi:10.1016/J.SURFCOAT.2016.12.080.

[21] A. Hatem, J. Lin, R. Wei, R.D. Torres, C. Laurindo, P. Soares, Tribocorrosion behavior of DLC-coated Ti-6Al-4V alloy deposited by PIID and PEMS+PIID techniques for biomedical applications, Surf. Coatings Technol. (2017). doi:10.1016/j.surfcoat.2017.07.004.

[22] T.M. Manhabosco, I.L. Müller, Tribocorrosion of diamond-like carbon deposited on Ti6Al4V, Tribol. Lett. 33 (2009) 193–197. doi:10.1007/s11249-009-9408-8.

[23] A. Erdemir, C. Bindal, G.R. Fenske, C. Zuiker, P. Wilbur, Characterization of transfer layers forming on surfaces sliding against diamond-like carbon, Surf. Coatings Technol. 86–87 (1996) 692–697. doi:10.1016/S0257-8972(96)03073-3.

[24] S.J. Bull, Tribology of carbon coatings: DLC, diamond and beyond, Diam. Relat. Mater. 4 (1995) 827–836. doi:10.1016/0925-9635(94)05325-1.

[25] B. McEntire, R. Lakshminarayanan, Coated implants and related methods, Patent No.: US 9,051,639 B2, 2015.

[26] J. Xu, G.D. Wang, X. Lu, L. Liu, P. Munroe, Z.H. Xie, Mechanical and corrosion-resistant properties of Ti-Nb-Si-N nanocomposite films prepared by a double glow discharge plasma technique, Ceram. Int. 40 (2014) 8621–8630. doi:10.1016/j.ceramint.2014.01.079.

[27] Y.H. Yoo, D.P. Le, J.G. Kim, S.K. Kim, P. Van Vinh, Corrosion behavior of TiN, TiAlN, TiAlSiN thin films deposited on tool steel in the 3.5 wt.% NaCl solution, Thin Solid Films. 516 (2008) 3544–3548. doi:10.1016/j.tsf.2007.08.069.

[28] D.K. Lee, D.S. Kang, J.H. Suh, C.G. Park, K.H. Kim, Synthesis and mechanical evaluation of quaternary Ti-Cr-Si-N coatings deposited by a hybrid method of arc ion plating and sputtering techniques, Surf. Coatings Technol. 200 (2005) 1489–1494. doi:10.1016/j.surfcoat.2005.08.023.

[29] R. Wei, C. Rincon, E. Langa, Q. Yang, Microstructure and tribological performance of nanocomposite Ti–Si–C–N coatings deposited using hexamethyldisilazane precursor, J. Vac. Sci. Technol. A Vacuum, Surfaces, Film. 28 (2010) 1126. doi:10.1116/1.3463709.

[30] E. Thangavel, S. Lee, K.S. Nam, J.K. Kim, D.G. Kim, Synthesis and characterization of Ti-Si-C-N nanocomposite coatings prepared by a filtered vacuum arc method, Appl. Surf. Sci. 265 (2013) 60–65. doi:10.1016/j.apsusc.2012.10.107.

[31] R. Wei, E. Langa, C. Rincon, J.H. Arps, Deposition of thick nitrides and carbonitrides for sand erosion protection, Surf. Coatings Technol. 201 (2006) 4453–4459. doi:10.1016/j.surfcoat.2006.08.091.

[32] J. Lin, R. Wei, D.C. Bitsis, P.M. Lee, Development and evaluation of low friction

TiSiCN nanocomposite coatings for piston ring applications, Surf. Coatings Technol. 298 (2016) 121–131. doi:10.1016/j.surfcoat.2016.04.061.

[33] Y. Yuan, Z. Qin, D.H. Yu, C.Y. Wang, J. Sui, H. Lin, Q. Wang, Relationship of microstructure, mechanical properties and hardened steel cutting performance of TiSiN-based nanocomposite coated tool, J. Manuf. Process. 28 (2017) 399–409. doi:10.1016/j.jmapro.2017.07.007.

[34] H. Xu, X. Nie, R. Wei, Tribological behavior of a TiSiCN coating tested in air and coolant, Surf. Coatings Technol. 201 (2006) 4236–4241. doi:10.1016/j.surfcoat.2006.08.066.

[35] A.A. a Onoprienko, V.I. V Ivashchenko, S.N.N. Dub, O.Y.Y. Khyzhun, I.I.I. Timofeeva, Microstructure and mechanical properties of hard Ti–Si–C–N films deposited by dc magnetron sputtering of multicomponent Ti/C/Si target, Surf. Coatings Technol. 205 (2011) 5068–5072. doi:10.1016/j.surfcoat.2011.05.009.

[36] S.L. Ma, D.Y. Ma, Y. Guo, B. Xu, G.Z. Wu, K.W. Xu, P.K. Chu, Synthesis and characterization of super hard, self-lubricating Ti-Si-C-N nanocomposite coatings, Acta Mater. 55 (2007) 6350–6355. doi:10.1016/j.actamat.2007.07.046.

[37] Y. Guo, S. Ma, K. Xu, Effects of carbon content and annealing temperature on the microstructure and hardness of super hard Ti-Si-C-N nanocomposite coatings prepared by pulsed d.c. PCVD, Surf. Coatings Technol. 201 (2007) 5240–5243. doi:10.1016/j.surfcoat.2006.07.122.

[38] S. Vepřek, S. Reiprich, L. Shizhi, Superhard nanocrystalline composite materials: The TiN/Si3N4 system, Appl. Phys. Lett. 66 (1995) 2640. doi:10.1063/1.113110.

[39] W. Li, P. Liu, Z. Xue, F. Ma, K. Zhang, X. Chen, R. Feng, P.K. Liaw, Microstructures, mechanical behavior and strengthening mechanism of TiSiCN nanocomposite films, Sci. Rep. 7 (2017) 1–10. doi:10.1038/s41598-017-02186-1.

[40] J.H. Jeon, S.R. Choi, W.S. Chung, K.H. Kim, Synthesis and characterization of quaternary Ti-Si-C-N coatings prepared by a hybrid deposition technique, Surf. Coatings Technol. 188–189 (2004) 415–419. doi:10.1016/j.surfcoat.2004.08.042.

[41] D. V. Shtansky, E. a. Levashov, a. N. Sheveiko, J.J. Moore, Synthesis and characterization of Ti-Si-C-N films, Metall. Mater. Trans. A. 30 (1999) 2439–2447. doi:10.1007/s11661-999-0252-0.

[42] Y. Wang, J. Li, C. Dang, Y. Wang, Y. Zhu, Influence of carbon contents on the structure and tribocorrosion properties of TiSiCN coatings on Ti6Al4V, Tribol. Int. 109 (2017) 285–296. doi:10.1016/j.triboint.2017.01.002.

[43] A.O. Eriksson, N. Ghafoor, J. Jensen, L.Å. Näslund, M.P. Johansson, J. Sjölen, M. Odén, L. Hultman, J. Rosen, Arc deposition of Ti-Si-C-N thin films from binary and ternary cathodes - Comparing sources of C, Surf. Coatings Technol. 213 (2012) 145–154. doi:10.1016/j.surfcoat.2012.10.038.

[44] A.M. Abd El-Rahman, R. Wei, A comparative study of conventional magnetron sputter deposited and plasma enhanced magnetron sputter deposited Ti–Si–C–N

nanocomposite coatings, Surf. Coatings Technol. 241 (2014) 74–79. doi:10.1016/j.surfcoat.2013.08.049.

[45] C. Oliveira, R.E. Galindo, C. Palacio, L. Vázquez, A. Espinosa, B.G. Almeida, M. Henriques, S. Calderon V, S. Carvalho, Influence of the surface morphology and microstructure on the biological properties of Ti-Si-C-N-O coatings, Thin Solid Films. 518 (2010) 5694–5699. doi:10.1016/j.tsf.2010.05.050.

[46] R. Wei, Plasma enhanced magnetron sputter deposition of Ti-Si-C-N based nanocomposite coatings, Surf. Coatings Technol. 203 (2008) 538–544. doi:10.1016/j.surfcoat.2008.05.019.

[47] A.L. Patterson, The Scherrer Formula for X-Ray Particle Size Determination, Phys. Rev. 56 (1939) 978–982. doi:10.1103/PhysRev.56.978.

[48] P. Scherrer, Bestimmung der inneren Struktur und der Größe von Kolloidteilchen mittels Röntgenstrahlen, in: Kolloidchem. Ein Lehrb., Springer Berlin Heidelberg, Berlin, Heidelberg, 1912: pp. 387–409. doi:10.1007/978-3-662-33915-2_7.

[49] ASTM C1624-05(2015), Standard Test Method for Adhesion Strength and Mechanical Failure Modes of Ceramic Coatings by Quantitative Single Point Scratch Testing, ASTM International, West Conshohocken, PA, 2015. doi:10.1520/C1624-05R15.

[50] Q. Li, F.Q. Jiang, Y.X. Leng, R.H. Wei, N. Huang, Microstructure and tribological properties of Ti(Cr)SiCN coating deposited by plasma enhanced magnetron sputtering, Vacuum. 89 (2013) 168–173. doi:10.1016/j.vacuum.2012.03.053.

[51] Y. Yao, J. Li, Y. Wang, Y. Ye, L. Zhu, Influence of the negative bias in ion plating on the microstructural and tribological performances of Ti-Si-N coatings in seawater, Surf. Coatings Technol. 280 (2015) 154–162. doi:10.1016/j.surfcoat.2015.09.005.

[52] B.J. Burrow, A.E. Morgan, R.C. Ellwanger, A correlation of Auger electron spectroscopy, x- ray photoelectron spectroscopy, and Rutherford backscattering spectrometry measurements on sputter- deposited titanium nitride thin films, J. Vac. Sci. Technol. A Vacuum, Surfaces, Film. 4 (1986) 2463–2469. doi:10.1116/1.574092.

[53] N.C. Saha, H.G. Tompkins, Titanium nitride oxidation chemistry: An x- ray photoelectron spectroscopy study, J. Appl. Phys. 72 (1992) 3072–3079. doi:10.1063/1.351465.

[54] S. Badrinarayanan, S. Sinha, A.B. Mandale, XPS studies of nitrogen ion implanted zirconium and titanium, J. Electron Spectros. Relat. Phenomena. 49 (1989) 303–309. doi:10.1016/0368-2048(89)85018-2.

[55] C. Dang, J. Li, Y. Wang, J. Chen, Structure, mechanical and tribological properties of self-toughening TiSiN/Ag multilayer coatings on Ti6Al4V prepared by arc ion plating, Appl. Surf. Sci. 386 (2016) 224–233. doi:10.1016/J.APSUSC.2016.06.024.

[56] J.A. Taylor, G.M. Lancaster, J.W. Rabalais, Chemical reactions of N 2+ ion beams with group IV elements and their oxides, J. Electron Spectros. Relat. Phenomena. 13 (1978) 435–444. doi:10.1016/0368-2048(78)85047-6.

[57] R. Alfonsetti, G. De Simone, L. Lozzi, M. Passacantando, P. Picozzi, S. Santucci, SiOx surface stoichiometry by XPS: A comparison of various methods, Surf. Interface Anal. 22 (1994) 89–92. doi:10.1002/sia.740220122.

[58] H. Ihara, Y. Kumashiro, A. Itoh, K. Maeda, Some Aspects of ESCA Spectra of Single Crystals and Thin Films of Titanium Carbide, Jpn. J. Appl. Phys. 12 (1973) 1462–1463. doi:10.1143/JJAP.12.1462.

[59] A.A. Galuska, J.C. Uht, N. Marquez, Reactive and nonreactive ion mixing of Ti films on carbon substrates, J. Vac. Sci. Technol. A Vacuum, Surfaces, Film. 6 (1988) 110–122. doi:10.1116/1.574992.

[60] J. Filik, P.W. May, S.R.J. Pearce, R.K. Wild, K.R. Hallam, XPS and laser Raman analysis of hydrogenated amorphous carbon films, Diam. Relat. Mater. 12 (2003) 974–978. doi:10.1016/S0925-9635(02)00374-6.

[61] X.B. Yan, T. Xu, S.R. Yang, H.W. Liu, Q.J. Xue, Characterization of hydrogenated diamond-like carbon films electrochemically deposited on a silicon substrate, J. Phys. D. Appl. Phys. 37 (2004) 2416–2424. doi:10.1088/0022-3727/37/17/012.

[62] T.Y. Leung, W.F. Man, P.K. Lim, W.C. Chan, F. Gaspari, Determination of the sp 3 / sp 2 ratio of a-C : H by XPS and XAES, 254 (1999) 156–160.

[63] A. Grill, Diamond-like carbon: state of the art, Diam. Relat. Mater. 8 (1999) 428–434. doi:10.1016/S0925-9635(98)00262-3.

[64] J. Robertson, Diamond-like amorphous carbon, Mater. Sci. Eng. R Reports. 37 (2002) 129–281. doi:10.1016/S0927-796X(02)00005-0.

[65] A. Snis, S.F. Matar, Electronic density of states, 1 s core-level shifts, and core ionization energies of graphite, diamond, C 3 N 4 phases, and graphitic C 11 N 4, Phys. Rev. B. 60 (1999) 10855–10863. doi:10.1103/PhysRevB.60.10855.

[66] G.M. Ingo, N. Zacchetti, XPS investigation on the growth model of a-SiNx and silicon and nitrogen chemical bondings, High Temp. Sci. 28 (1988) 137–151.

[67] E. Galvanetto, F.P. Galliano, F. Borgioli, U. Bardi, A. Lavacchi, XRD and XPS study on reactive plasma sprayed titanium–titanium nitride coatings, Thin Solid Films. 384 (2001) 223–229. doi:10.1016/S0040-6090(00)01871-X.

[68] J. Lin, R. Wei, F. Ge, Y. Li, X. Zhang, F. Huang, M. Lei, TiSiCN and TiAlVSiCN nanocomposite coatings deposited from Ti and Ti-6Al-4V targets, Surf. Coatings Technol. 336 (2018) 106–116. doi:10.1016/j.surfcoat.2017.10.009.

[69] E.A. Levashov, D. V. Shtansky, Multifunctional nanostructured films, Russ. Chem. Rev. 76 (2007) 463–470. doi:10.1070/RC2007v076n05ABEH003679.

[70] A.D. (Alexander D.. Pogrebnjak, V.M. Beresnev, Nanocoatings nanosystems nanotechnologies, Bentham Books, 2012. https://books.google.com.br/books?hl=pt-BR&lr=&id=vRkyDgAAQBAJ&oi=fnd&pg=PP1&ots=xVcCrE5Kua&sig=HMzv-ln5ggH2Pm8_qZQCip-Acpw#v=onepage&q&f=true (accessed January 25, 2018).

[71] A. Leyland, A. Matthews, On the significance of the H/E ratio in wear control: A nanocomposite coating approach to optimised tribological behaviour, Wear. 246 (2000) 1–11. doi:10.1016/S0043-1648(00)00488-9.

[72] J. Musil, F. Kunc, H. Zeman, H. Poláková, Relationships between hardness, Young's modulus and elastic recovery in hard nanocomposite coatings, Surf. Coatings Technol. 154 (2002) 304–313. doi:10.1016/S0257-8972(01)01714-5.

[73] J. Musil, M. Jirout, Toughness of hard nanostructured ceramic thin films, Surf. Coatings Technol. 201 (2007) 5148–5152. doi:10.1016/J.SURFCOAT.2006.07.020.

[74] S.J. Bull, E. G.-Berasetegui E., An overview of the potential of quantitative coating adhesion measurement by scratch testing, Tribol. Interface Eng. Ser. 51 (2006) 136–165. doi:10.1016/S0167-8922(06)80043-X.

[75] S.J. Bull, Failure modes in scratch adhesion testing, Surf. Coatings Technol. 50 (1991) 25–32. doi:10.1016/0257-8972(91)90188-3.

[76] V. Schroeder, C.J. Gilbert, R.O. Ritchie, Comparison of the corrosion behavior of a bulk amorphous metal, Zr41.2Ti13.8Cu12.5Ni10Be 22.5, with its crystallized form, Scr. Mater. 38 (1998) 1481–1485. doi:10.1016/S1359-6462(98)00089-X.

[77] J.C.M. de Souza, Biotribocorrosion behavior of titanium in simulated oral environments, J. Chem. Inf. Model. 53 (2009) 1689–1699. doi:10.1017/CBO9781107415324.004.

[78] B.S. Bal, M.N. Rahaman, Orthopedic applications of silicon nitride ceramics, Acta Biomater. 8 (2012) 2889–2898. doi:10.1016/j.actbio.2012.04.031.

5 PUBLICAÇÕES E APRESENTAÇÕES EM CONGRESSO

5.1 PUBLICAÇÕES

- HATEM, A.; LIN, J.; WEI, R.; TORRES, R. D.; LAURINDO, C.; SOARES, P. Tribocorrosion behavior of DLC-coated Ti-6Al-4V alloy deposited by PIID and PEMS+PIID techniques for biomedical applications. **Surface and Coatings Technology**, v. 332, p. 223–232, 2017.

- HATEM, A.; REALI, L; LIN, J.; WEI, R.; TORRES, R. D.; LAURINDO, C.; SOARES, P. Adhesion evaluation of nanostructured coatings on titanium alloy for biomedical applications. **Conference: 24th ABCM International Congress of Mechanical Engineering**, 2017. DOI: 10.26678/ABCM.COBEM2017.COB17-2383

- HATEM, A.; LIN, J.; WEI, R.; TORRES, R. D.; LAURINDO, C.; DE SOUZA, G. B.; SOARES, P. Tribocorrosion behavior of low friction TiSiCN nanocomposite coatings deposited on titanium alloy for biomedical applications. **Surface and Coatings Technology**, v. 347, p. 1–12, 2018.

5.2 APRESENTAÇÕES EM CONGRESSO

9º COLAOB – Congresso Latino-Americano de Orgãos Artificiais e Biomateriais:

- HATEM, A., LIN, J., WEI, R., TORRES, R. D., LAURINDO, C., & SOARES, P. (2016). Tribological properties of DLC films on titanium alloys deposited by PIID and PEMS+PIID techniques. Poster presented at the **9th Latin American Congress on Artificial Organs and Biomaterials**, Foz do Iguaçu, PR, Brazil.

44TH ICMCTF – International Conference on Metallurgical Coatings and Thin Films:

- HATEM, A., LIN, J., WEI, R., TORRES, R. D., LAURINDO, C., & SOARES, P. (2017). Tribocorrosion Behaviour of Nanocomposite TiSiCN Coatings Tested in PBS Solution. Poster presented at the **44th ICMCTF - International Conference on Metallurgical Coatings and Thin Films**, San Diego, CA, USA.

- HATEM, A., LIN, J., WEI, R., TORRES, R. D., LAURINDO, C., & SOARES, P. (2017). Tribocorrosion Behaviour of DLC-Coated Ti-6Al-4V Alloy Deposited by PIID and PEMS+PIID Techniques for Biomedical Applications. Presented at the **44th ICMCTF - International Conference on Metallurgical Coatings and Thin Films**, San Diego, CA, USA.

24TH COBEM – ABCM International Congress of Mechanical Engineering:

- HATEM, A., LIN, J., WEI, R., TORRES, R. D., LAURINDO, C., & SOARES, P. (2017). Adhesion evaluation of nanostructured coatings on titanium alloy for biomedical applications. Presented at the **24th COBEM - ABCM International Congress of Mechanical Engineering**, Curitiba, PR, Brazil.

6 CONSIDERAÇÕES FINAIS

Este trabalho teve como objetivo geral a caracterização tribocorrosiva, mecânica e estrutural de revestimentos nanoestruturados depositados em liga de titânio ASTM F136 propostos para aplicações biomédicas. De forma geral, os revestimentos estudados apresentaram expressiva redução da taxa de desgaste durante os testes de tribocorrosão em PBS quando comparados a liga de titânio não revestida. Os resultados demonstraram que a performance tribocorrosiva destes revestimentos está ligada a um conjunto de fatores, sendo os principais, um baixo coeficiente de atrito (COF) aliado a elevada resistência mecânica dos revestimentos, em particular, valores mais altos dos índices H/E e H^3/E^2. A formação de uma camada de transferência de material a partir de regiões de carbono amorfo se mostrou eficaz na redução do coeficiente de atrito, porém, ao mesmo tempo, acentuou a taxa de desgaste devido sua baixa resistência às forças cisalhantes. Desta forma o equilíbrio entre estas regiões com estruturas de maior resistência mecânica apresentou condições ideais e de menores taxas de desgaste nos testes de tribocorrosão. De fato, estes fatores estão intrinsicamente relacionados a estrutura obtida em cada um dos revestimentos durante sua deposição. Dentre os revestimentos estudados, o nanocompóstio TiSiCN com menor tamanho de nanocristal obteve a menor taxa de desgaste.

Os objetivos específicos deste trabalho foram atendidos, e as principais conclusões estão respectivamente apresentadas abaixo:

- A fração de ligações sp²/sp³ presentes nos revestimentos DLC demonstraram forte correlação com às propriedades mecânicas e de adesão dos revestimentos e a formação de camada de transferência de carbono durante os testes de tribocorrosão. Os resultados demonstraram que uma maior a quantidade de ligações sp² contribui para um coeficiente de atrito menor ao longo do movimento de deslizamento recíproco sob PBS, porém não necessariamente para a menor taxa de desgaste. O que sugere que a formação da camada de transferência de carbono é beneficiada por estas ligações, sendo rápida e recorrente no par tribológico, porém apresentando fraca resistência ao cisalhamento que acelera o processo de desgaste destas regiões presentes no revestimento. Entretanto altas quantidades de ligações sp³, introduzem tensões residuais maiores aos revestimentos que prejudicam sua adesão sob o substrato, representadas pelas delaminações e baixas cargas críticas verificadas nos testes de adesão realizados. Desta maneira tornou-se evidente a necessidade de equilíbrio e controle da fração de ligações sp²/sp³ para a

obtenção de um comportamento tribocorrosivo ideal em revestimentos DLC depositados sob a liga de titânio estudada.

- As quantidades de carbono e silício presentes nos revestimentos Ti(Si)CN se apresentaram como refinadores da estrutura do material, proporcionando uma diminuição diretamente proporcional ao tamanho dos nanocristais de Ti(C)N contidos na microestrutura. Isto se deve ao fato do silício estar presente na matriz amorfa de Si_3N_4 circundante aos nanocristais e o carbono excedente se apresentar em regiões de carbono amorfo dispersos na microestrutura. Essa diminuição atribui melhora nas propriedades mecânicas e nos índices H/E e H^3/E^2, e por consequência no comportamento tribocorrosivo dos revestimentos nos testes realizados com as quantidades dos elementos (Si,C) examinadas. A melhora da performance tribocorrosiva se demonstrou aparente pela ausência de delaminações nos revestimentos com valores elevados de Silício e Carbono, sendo o melhor resultado obtido na amostra com o menor tamanho de nanocristal. Um aumento singular na quantidade de carbono apresentou resultados com taxa de degaste levemente superior a níveis com menos carbono e mesma quantidade de silício. Isto sugere um desgaste acentuado das regiões de carbono amorfo com baixa resistência ao cisalhamento, resultado similar ao observado em revestimentos DLC com alta quantidade de ligações sp^2. Por fim, elevadas quantidades de carbono e silício demonstraram importantes no refino da microestrutura dos revestimentos nanocompósitos Ti(Si)CN e desta maneira fundamentais para a melhora do seu comportamento tribocorrosivo.

- Os índices H/E e H^3/E^2 se demonstraram intrinsicamente ligado com a resistência ao desgaste dos revestimentos DLC e Ti(Si)CN submetidos ao teste de tribocorrosão. As menores taxas de desgaste foram verificadas nos revestimentos com maiores valores destes índices. De fato, os índices H/E e H^3/E^2 são geralmente descritos como a resistência do material à deformação elástica e plástica respectivamente. Desta maneira maiores índices indicam uma diminuição nos deslocamentos relativos dos materiais presentes no sistema do filme junto ao substrato, o que previne trincas, delaminações e sugere a diminuição do desgaste abrasivo. Desta maneira, o estudo demonstrou que maiores valores dos índices de H/E e H^3/E^2 devem ser visados na obtenção

de revestimentos DLC e Ti(Si)CN depositados sob liga de titânio com melhor performance tribocorrosiva.

- O potencial de circuito aberto (OCP), o coeficiente de atrito (COF) e a taxa de desgaste foram alvo de estudo durante os testes de tribocorrosão das amostras revestidas e comparadas com uma amostra de controle de liga de titânio não revestida. A comparação do OCP das amostras revestidas com a amostra de controle se demonstrou importante na identificação de pequenas delaminações do revestimento, mesmo quando apenas entre as camadas de adesão e o filme, como no caso das amostras de Ti(Si)CN até 3.0 sccm de TMS. O COF revelou a atuação da camada de transferência de material ao longo de todo o teste de tribocorrosão com uma inclinação no sentido de menores valores de COF com a distância, diferentemente do observado na amostra de controle. Isto explicou a drástica diminuição de desgaste por abrasão observado nas imagens das trilhas de desgaste. As comparações das taxas de desgaste entre revestimentos demonstraram que menores valores de COF não necessariamente resultaram em menores taxas de desgaste. Estas observações aliadas aos demais testes realizados sugeriram que as regiões de carbono amorfo atuam na lubrificação do par tribológico porém também acentuam o desgaste devido a constante remoção e adesão deste material no interior da trilha de desgaste. Por fim, estas comparações foram fundamentais para o entendimento dos mecanismos responsáveis pela performance tribocorrosiva dos revestimentos DLC e Ti(Si)CN depositados sob a liga de titânio estudada.

Ainda se ressalva que as pressões de contato de hertz utilizadas neste estudo são equivalentemente muito superiores a aquelas submetidas às próteses em uso. Estas condições foram adotadas para viabilizar os testes em bancada, bem como impor o aparecimento de falhas nos revestimentos afim de uma comparação qualitativa entre as amostras.

As sugestões para trabalhos futuros incluem o desenvolvimento de uma bancada com movimento simulado específico para o implante proposto; o estudo da bioatividade e citotoxicidade do material destes revestimentos; o estudo das tensões residuais nos revestimentos, especialmente no DLC; e a análise do meio corrosivo após o teste de tribocorrosão para a identificação das partículas de desgaste.

REFERÊNCIAS

DESAI, S.; BIDANDA, B.; BÁRTOLO, P. Metallic and Ceramic Biomaterials: Current and Future Developments. *In*: BÁRTOLO, P.; BIDANDA, B. (Eds.). . **Bio-Materials and Prototyping Applications in Medicine**. 1. ed. [s.l.] Springer US, 2008. p. 1–14.

ERDEMIR, A.; BINDAL, C.; FENSKE, G. R.; ZUIKER, C.; WILBUR, P. **Characterization of transfer layers forming on surfaces sliding against diamond-like carbonSurface and Coatings Technology**, 1996.

GEETHA, M.; SINGH, A. K.; ASOKAMANI, R.; GOGIA, A. K. Ti based biomaterials, the ultimate choice for orthopaedic implants - A review. **Progress in Materials Science**, v. 54, n. 3, p. 397–425, 2009.

GOPAL, V.; CHANDRAN, M.; RAO, M. S. R.; MISCHLER, S.; CAO, S.; MANIVASAGAM, G. Tribocorrosion and electrochemical behaviour of nanocrystalline diamond coated Ti based alloys for orthopaedic application. **Tribology International**, v. 106, p. 88–100, 2017.

GRILL, A. Diamond-like carbon: state of the art. **Diamond and Related Materials**, v. 8, n. 2–5, p. 428–434, 1999.

HALLAB, N. J.; ANDERSON, S.; CAICEDO, M.; BRASHER, A.; MIKECZ, K.; JACOBS, J. J. Effects of soluble metals on human peri-implant cells. **Journal of Biomedical Materials Research Part A**, v. 74A, n. 1, p. 124–140, 1 jul. 2005.

HAUERT, R. DLC Films in Biomedical Applications. *In*: **Tribology of Diamond-Like Carbon Films**. Boston, MA: Springer US, 2008. p. 494–509.

HERBERTS, P.; MALCHAU, H. Long-term registration has improved the quality of hip replacement: a review of the Swedish THR Register comparing 160,000 cases. **Acta orthopaedica Scandinavica**, v. 71, n. 2, p. 111–121, 2000.

KURTZ, S.; ONG, K.; LAU, E.; MOWAT, F.; HALPERN, M. Projections of primary and revision hip and knee arthroplasty in the United States from 2005 to 2030. **The Journal of bone and joint surgery (Am)**, v. 89, n. 4, p. 780–5, 2007.

MANHABOSCO, T. M.; MÜLLER, I. L. Tribocorrosion of diamond-like carbon deposited on Ti6Al4V. **Tribology Letters**, v. 33, n. 3, p. 193–197, 2009.

MCENTIRE, B.; LAKSHMINARAYANAN, R. **Coated implants and related methods**United States, 2015.

RAPHEL, J.; HOLODNIY, M.; GOODMAN, S. B.; HEILSHORN, S. C. Multifunctional coatings to simultaneously promote osseointegration and prevent infection of orthopaedic implants. **Biomaterials**, v. 84, p. 301–314, 2016.

ROBERTSON, J. Diamond-like amorphous carbon. **Materials Science and Engineering: R: Reports**, v. 37, n. 4–6, p. 129–281, 2002.

ROBERTSSON, O.; KNUTSON, K.; LEWOLD, S.; LIDGREN, L. The Swedish Knee Arthroplasty Register 1975-1997: an update with special emphasis on 41,223 knees operated on in 1988-1997. **Acta orthopaedica Scandinavica**, v. 72, n. 5, p. 503–13, 2001.

SADOGHI, P.; LIEBENSTEINER, M.; AGREITER, M.; LEITHNER, A.; BÖHLER, N.; LABEK, G. Revision surgery after total joint arthroplasty: A complication-based analysis using worldwide arthroplasty registers. **Journal of Arthroplasty**, v. 28, n. 8, p. 1329–1332, 2013.

SARGEANT, A.; GOSWAMI, T. Hip implants: Paper V. Physiological effects. **Materials and Design**, v. 27, n. 4, p. 287–307, 2006.

SERLE, G. **John Monash: a biography**. Carlton, Victoria, Australia: Melbourne University Press in association with Monash University, 1982.

WANG, Y. Y. Y.; LI, J.; DANG, C.; WANG, Y. Y. Y.; ZHU, Y. Influence of carbon contents on the structure and tribocorrosion properties of TiSiCN coatings on Ti6Al4V. **Tribology International**, v. 109, n. October 2016, p. 285–296, 2017.

XU, H.; NIE, X.; WEI, R. Tribological behavior of a TiSiCN coating tested in air and coolant. **Surface and Coatings Technology**, v. 201, n. 7 SPEC. ISS., p. 4236–4241, 2006.